Journal of Materials Chemistry A

Accepted Manuscript

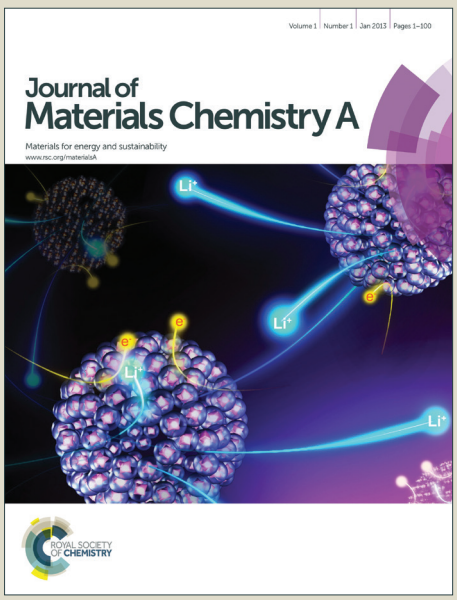

ROYAL SOCIETY OF CHEMISTRY

www.rsc.org/materialsA

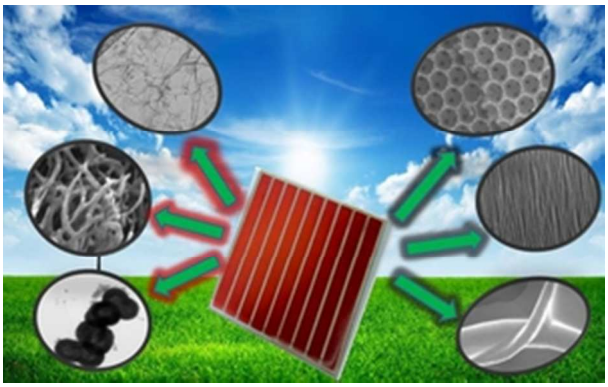

25x15mm (300 x 300 DPI)

The present manuscript analyzes the role of various carbon nanostructures in the photoanode and counter electrode of dye-sensitized solar cells.

Journal Name

ARTICLE

An in-depth Review on the Role of Carbon Nanostructures in Dye-sensitized Solar Cells

Received 00th January 20xx,
Accepted 00th January 20xx

DOI: 10.1039/x0xx00000x

www.rsc.org/

Murugesan Janani, Pillalamarri Srikrishnarka, Shantikumar V Nair and A. Sreekumaran Nair*

Dye-sensitized solar cells (DSSCs) are considered to be a promising, low-cost alternatives for the amorphous silicon solar cells. The major components of a DSC include a metal oxide (usually TiO_2), dye, electrolyte and a Pt- or carbon-deposited counter electrode. The photoexcited electrons from the dyes diffuse through the TiO_2 network and reach the counter electrode through an external circuit. However due to the trap-limited diffusion process, the electron collection efficiency is affected. Thus, for a hassale-free transport of electrons there is a need for additional electron transport channels. Further in order to reduce the overall cost of the device there is also a need for cheaper alternative counter electrodes in place of Pt. The 15th most abundant element in the earth's crust carbon and its allotropes with their outstanding catalytic activity and electrical conductivity proves to be a promising material to overcome all these shortcomings and demerits. The review presented below summarizes the up-to-date research efforts on the role of carbon nanostructures in DSSCs, the various synthetic strategies adopted their preparation and their photovoltaic performance. The review also includes a brief discussion about the role of carbon nanostructures in non- planar flexible wire shaped DSSC.

INTRODUCTION

HISTORY OF DYE SENSITIZED SOLAR CELLS

The history of the dye-sensitized solar cells (DSSCs) goes way back to 1873 when the German photochemist Vogel invented the first panchromatic film rendering the realistic black and white image by the dye sensitization of the silver halide emulsions leading to extended response into the infrared region.[1] Then in 1960 (Namba and Hishiki)[2] and Tributsch and Gerischer et al[3] worked on the sensitization of ZnO with chlorophyll as sensitizer. They found that upon the excitation of the dye, the excited electrons from the dye are injected into the conduction band of the semiconductor substrates. However the conversion efficiencies were poor owing to poor anchoring of the dyes on the semiconductor substrate. This was followed by the breakthrough experiments on the splitting of water on the TiO_2 by Fujishima and Honda that attracted the scientific community to the wide band gap material, TiO_2. In 1977, Spitler and Calvin proved that TiO_2 can be used instead of ZnO for DSCs.[4] This eventually led to the invention of dye sensitized solar cells in 1991 by Gräztel and his co-workers.[5]

The DSC invented by Gräztel is the third generation solar cell and it consists of a conducting glass plate usually fluorine-doped tin oxide (FTO) coated with TiO_2. The TiO_2 is sensitized with a dye. The most commonly used dyes are the ruthenium based dyes such as N3,[6] N719[7] and black dye.[8] The electrolyte usually contains I^-/I_3^- or cobalt-based redox couple and a counter electrode usually made of Platinum.

WORKING OF A DSSC:

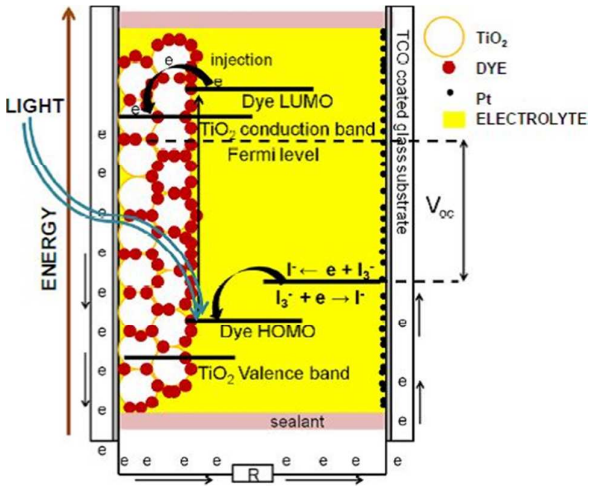

Figure 1: Schematic showing working of Dye sensitized Solar Cells.[22b]

When light is incident on the cell, the electrons from the highest occupied molecular orbital (HOMO) of the dye are excited to the lowest unoccupied molecular orbital (LUMO) of the dye. The electrons are then injected into the conduction band of TiO_2 which in turn are transferred to the conducting glass plate through trap-limited diffusion process. Thus the

Amrita Centre for Nanosciences and Molecular Medicine
Amrita Institute of Medical Sciences (AIMS)
Amrita Vishwa Vidyapeetham University
AIMS PO, Ponekkara, Kochi 682041, Kerala, India.
Email: sreekumarannair@aims.amrita.edu

role of the photoanode includes dye adsorption and charge transport. Meanwhile the oxidized dye is regenerated by the electrolyte. The electrolyte in turn is regenerated by the electrons reaching the counter electrode through the external circuit.

RECOMBINATION REACTIONS IN DSSC

The electron injection from the excited dye to the conduction band of the TiO_2 takes place in femto seconds and the regeneration of the oxidized dye takes place in micro second. The mesoporous TiO_2 network is mainly composed of nanocrystals of TiO_2 connected together. The electron transport mechanism through the TiO_2 network can be explained in two ways namely the electric field driven charge transport[9] and trap-limited diffusion process.[10] Since TiO_2 is not electronically doped and it is surrounded by the ions of the electrolyte, contribution by the electric field for the transport of the electrons through the TiO_2 network is negligible. Thus the main driving force for the migration of electrons through the dense TiO_2 network is mainly the diffusion process.[11] During the diffusion of the electrons through the TiO_2 network the electrons encounters three important interfaces namely TiO_2/dye/electrolyte interface, TiO_2/TiO_2 and FTO/TiO_2 interface. These interfaces act as electron trap centres where the electrons can undergo recombination. Since TiO_2 is mesoporous there are chances that the electrolyte can get accommodated in the space between the TiO_2 molecules in the TiO_2 film. So the electrons from the conduction band of the TiO_2 can recombine with the electrolyte. The electrons can also recombine with the oxidized dye. Thus these recombination reactions are called as the dark reactions. The Figure 2 summarizes the various recombination reactions that take place in DSSC.

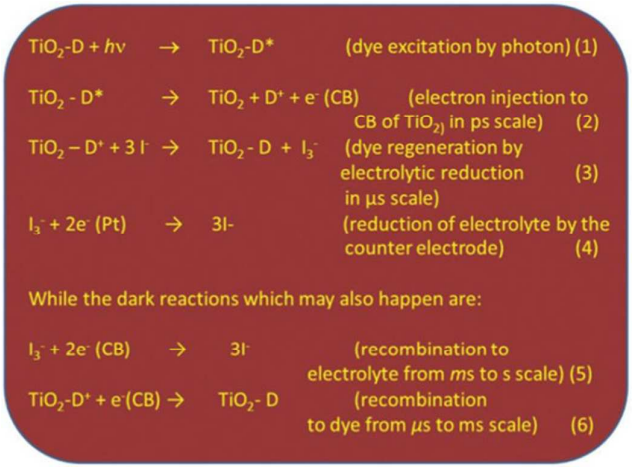

Fig. 2.Light and dark reactions in DSSC.[12]

Due to these recombination process all the electrons that are injected in the conduction band of the TiO_2 does not reach the FTO effectively and thus the overall efficiency of the cell is reduced. Thus the efficiency of the dye sensitized solar cell is solely dependent on the effective electron injection (high dye loading) and the competition between the effective transfer of electrons through the TiO_2 network without recombination and the regeneration of the dye.

ROLE OF NANOTECHNOLOGY:

Materials in their bulk size vary differently as their size reduces to nano regime. As size reduces, more and more atoms of the material are concentrated towards the surface thus leading to high surface energy. This high surface energy of the nano materials have been manipulated so as to use in various fields such as renewable energy, textiles, biomedical, health care, food and agriculture, electronics and environment. These nano materials fabricated, via top-down approach or bottom p approach, have low to zero impurities in them. This is one of the main reasons for utilizing these materials for drug delivery, imaging and also cancer therapy. By controlling the reaction conditions, various morphologies of nanomaterials can be obtained such as, 0D, 1D, 2D etc. particles and dots come under the 0D where in the particle synthesis is the simplest. Wires, rods, tubes, fibres come under 1D which have majority of applications in DSSC, photocatalysis, drug delivery etc. Sheets, flakes films generally come under 2D regime, wherein the fabrication slightly complicated than 0D/1D. anisotropic 3D structures, like flowers, tetrapods, tripods are difficult to fabricate on a large scale however they are being researched for photocatalysis, photoanodes in DSSC, batteries and supercapacitors.

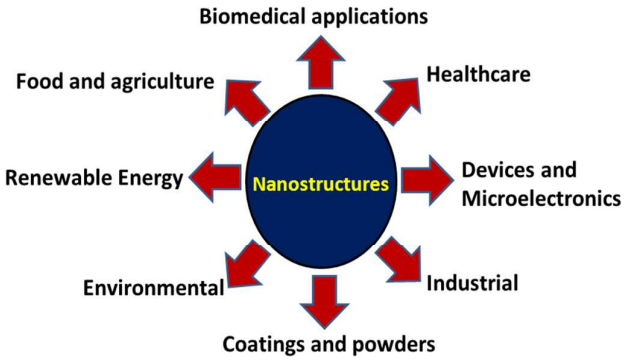

Fig. 3.Illustration showing application of Nanomaterials.

As the size reduces, the band gap increases which gives an additional advantage in imaging, storage and energy storage fields. As the band gap increases energy quantization phenomenon (Quantum confinement) takes place as observed in Quantum dots. This quantum confinement phenomenon has been applied in fields like cellular imaging and QDSC using quantum dots. Thus by tuning the morphology of the TiO_2 used in the DSSC, the recombination losses can be minimized and the performance of the device could be improved. Due to the high surface area of the nanostructures the dye loading capacity is greatly enhanced. This increased dye loading enhance the light harvesting efficiency and thus the overall performance of the cell. Several nanostructures with high surface area such as hollow spheres[13], micro beads[14], core-shell nanostructures,[15] etc. were widely investigated. However the zero-dimensional nanostructures do not provide a direct

pathway for the electrons to travel. Thus in order to provide a direct pathway for the electrons, one-dimensional nanostructures such as nanowires[16], nanorods[17], nanotubes[18] and nanofibers[19] of TiO_2 were employed in DSSC. However the one-dimensional nanostructures owing to their low internal surface area have poor dye loading which will pull down the light harvesting efficiency and in turn the overall performance of the cell. Thus in order to have the advantages of both the one-dimensional nanostructures and the high surface area of the zero-dimensional particles, TiO_2 particle-fiber composites[20-21] were employed. In addition to these morphologies several anisotropic morphologies were also used in DSSC. There is a detailed review article that describes the different anisotropic structures used in DSSC.[22] The collection efficiency of the electrons could also be improved by decreasing the electron path distance. Chapel et al. developed a photoanode that contains a transparent conductive nanoporous TiO_2 matrix coated with a thin layer of TiO_2.[23] Another significant way to prevent the recombination of electrons is to open an additional electron transport network in the TiO_2 film. This can be achieved by incorporating carbon nanostructures into the TiO_2 network.

THE CARBON NANOSTRUCTURES

The group 14 chemical element carbon with the atomic number 6 is widely distributed in nature in various forms and it is considered to be the 15th most abundant element in the earth's crust. Among the various allotropes of carbon diamond, graphite and amorphous carbon are the most common allotropes. In addition there are various allotropes of carbon having a wide range of dimensions varying from zero dimensional structures like fullerene, one-dimensional structures like carbon nanotubes, two-dimensional sheets like graphene to three-dimensional graphite synthesized in laboratory for various applications.

Table 1. Properties of Allotropes of Carbon.

Form of carbon	Hybridisation	Electron mobility (cm2/Vs)	Youngs Modulus	Thermal conductivity (W/m-K)
Diamond	sp^3	1800	1220GPa	25 W/cm-K
Graphite	sp^2	1.5*104 [24a]	0.795 TPa[28]	2200[24b]
Graphene	sp^2	2,00,000[25a]	1.06 TPa[29-30]	$(4.84*10^3)$ to $(5.50*10^3)$[25b]
CNT	sp^2	1,20,000[26a]	1.033-1.042 TPa[91]	6600[26b]
Fullerenes	sp^2	0.4-1[27]	53-69 GPa[32]	

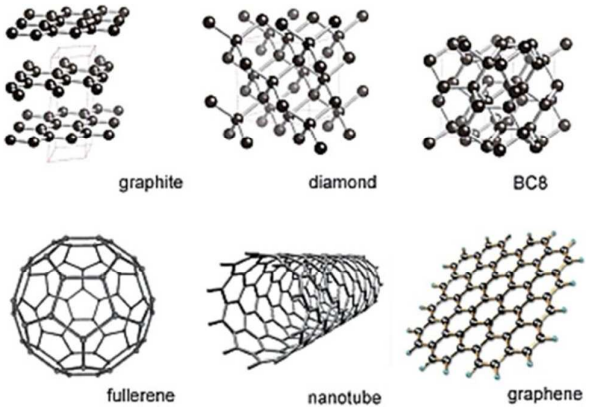

Fig. 4 Structure of various allotropes of carbon.[33]

These allotropes have different properties based on their structure. The table 1 summarizes the properties of various allotropes of carbon.

Due to the high electron mobility and conductivity, these carbon materials such as graphite[34], carbon black[35], mesoporous carbon[36], carbon nanotubes[37-39], and graphene[40-42] have a great deal of applications in optoelectronic devices. Among them graphene is a monolayer of sp^2 hybridized carbon atoms tightly packed into a two-dimensional honey-comb network[43] and it is the building block of all other allotropes of carbon. The charge carriers in graphene behave as massless Dirac fermions[44-47] exhibiting quantum hall effect[46-47] and ambipolar electric field effect.[44] Due to long range π interactions, they exhibit unique thermal, electrical and mechanical properties[48] and have high electron mobility of 15000c m^2/V.s at room temperature. Thus they found a lot of applications in nanoelectronics[49-53] batteries, solar cells, photocatalysis[54], etc.

The carbon nanotubes (CNT) are formed when a layer of graphene is rolled and it was first observed by Iijima. These CNTs are either single walled or double walled or multiwalled depending on the number of graphene sheets that are rolled to form the nanoscale CNTs.[55]

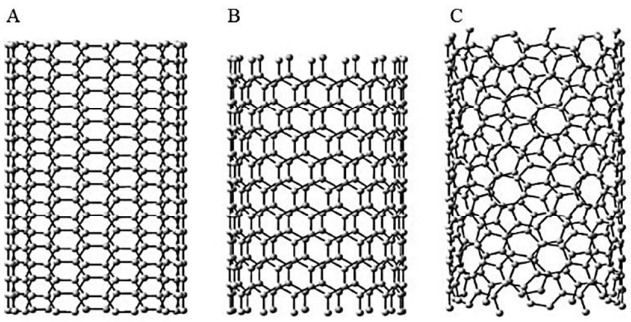

Fig. 5.A) CNT arm chair, B) CNT zig-zag, C) CNT chiral.[56]

In addition, depending on the chiral angle in which they are rolled-up, a number of structures like zig-zag, arm chair, chiral exist.[55] Based on the diameter of the CNTs and the helicity of the arrangement of the graphite ring, the CNTs are either

metallic or semiconducting. By joining different CNTs, molecular wires with unique mechanical, electrical, magnetic and optical properties are obtained.[57-58] Due to these unique properties, the CNTs have potential applications in single molecular transistors,[59] SEM tips,[60] gas and electrochemical storage,[61] electron field emitting flat panel displays[62] and sensors.[63] Further the addition of graphene as reinforcement enhances the electrical, mechanical and optical properties.[64-65]

CHARACTERISATION OF DSSC

The standard method to measure the performance of the solar cell is to measure its current density-voltage characteristics. A light with a well-defined spectrum and intensity usually AM 1.5 G is illuminated on the solar cell and the corresponding *J-V* characteristics are measured. From the *J-V* plot several parameters such as the open-circuit voltage, short-circuit current, fill-factor, maximum power density and photovoltaic conversion efficiency can be measured.

Open-circuit voltage (V_{oc}):

It is the maximum potential that could be drawn from the cell when there is no current. It is the potential difference of the cell when I=0 and r→∞. It is the measure of the potential difference between the Fermi level of the TiO_2 and the redox potential of the electrolyte.

Short-circuit current (I_{sc}):

It is the measure of the net effective current produced in the cell neglecting the current that is produced under dark condition.

$$J_{sc} = J_{sc}\text{-}J_{dark}$$

The short circuit current is dependent on the light harvesting efficiency and it is given as

$$LHE = 1 - 10^{-\Gamma\sigma(\lambda)}$$

Where,

Γ - No. of moles of sensitizer per square cm.

σ – Absorption cross section.

Fill-factor (FF):

It is the measure of the deviation of the behaviour of the actual cell from the ideal cell. It is defined as the ratio of the maximum power to the product of the V_{oc} and I_{sc}.

$$FF = \frac{I_{\max} V_{\max}}{I_{sc} V_{oc}}$$

The photovoltaic conversion efficiency is defined as the ratio of the maximum power delivered to that of the incident power.

$$\eta = \frac{P_{\max}}{P_{in}} = \frac{V_{oc} I_{sc} FF}{P_{in}}$$

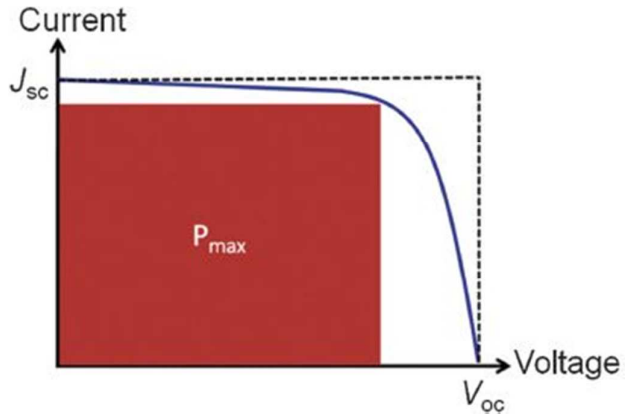

Fig. 6. Current- voltage characteristics of a typical DSSC. [22]

THE CARBON NANOSTRUCTURES/TiO_2 COMPOSITES FOR DSSC

There are different ways by which carbon nanostructures/TiO_2 composites could be made. In this review we explain about the various methods that are adopted for the synthesis of carbon nanostructures/TiO_2 composites and their photovoltaic performance.

CARBON NANOTUBE/TiO_2 COMPOSITES

Jung et al. were the first group to incorporate single walled carbon nanotubes (SW-CNT) into TiO_2 to facilitate the electron transport through the TiO_2 film and have shown 50% enhancement in the short-circuit current density.[66] However since the distribution of TiO_2 on the SW-CNT was irregular Kim et al. used acid treated multiwalled CNTs. The treatment of the CNTs with H_2SO_4 and HNO_3 introduces carboxylic acid groups on the surfaces of the CNTs which facilitate better adhesion of TiO_2 on the CNTs. The increase in the efficiency is due to the fact that, the rutile form of TiO_2 have superior light scattering property due to its high refractive index than the anatase form and also the increase in the interconnection among the TiO_2 particles when acid treated MW-CNTs are added, which blocks the surface electron trap sites.[67]

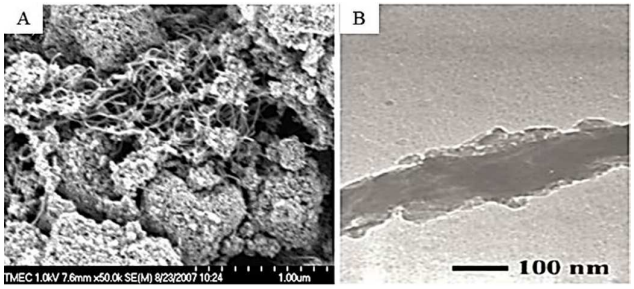

Fig. 7.A. FE-SEM image of MW-CNT/TiO_2 [68] and B. TEM image of MW-CNT/TiO_2 [67]

Sawatsuk et al. mixed multiwalled carbon nanotubes (MWCNT) and the TiO_2 powder directly and reported an efficiency of 10.29% with about 0.025wt% of MWCNT.[68] Lee et al. synthesized multiwalled CNT-TiO_2 composite in which TiO_2 was

made by sol-gel method and the MWCNTs are pre-processed with COOH groups. The multiwalled CNTs are generally hydrophobic in nature. However the oxidation of MWCNT with H_2O_2 makes it hydrophilic by the generation of the carboxylic acid group on the CNT. An overall efficiency of 4.97% was reported for 0.1 wt% of CNTs.[69]

The ruthenium dye that is used in DSSC anchors on to the metal oxide i.e. TiO_2 and not onto the surface of the carbon nanotubes. Thus if the mass density of the metal oxide is less, the active dye adsorption sites decreases. Thus if the metal oxide is not immobilized uniformly on the surface of the CNT, the total amount of the dye loaded will be poor, thereby reducing the light harvesting efficiency. In order to overcome this demerit and improve the binding between TiO_2 and CNTs, Jang et al. treated the CNTs with concentrated H_2SO_4 and HNO_3 which resulted in the introduction of –COOH groups on the surface of the CNTs. The presence of these –COOH groups on the CNT surface facilitate better adhesion between CNT and TiO_2. The acid treated single walled CNTs (a-SWCNT) were used in two ways. In the first case a-SWCNTs were incorporated into the TiO_2 films to improve the charge transfer in DSSC and the solar cell fabricated showed 25% increase in the J_{sc} than the one without the CNTs. In the second case, the dye molecules were anchored onto the a-SWCNT and they were introduced at the TiO_2/electrolyte interface where the a-SWCNT acts as light scattering centres. In this case V_{oc} increases whereas the J_{sc} remains constant. The increase in V_{oc} implies the reduction of the dark current and the increase is also attributed to the negative shift of the conduction band edge of the TiO_2 due to the basicity of the TiO_2 surface due to the –NH groups of the dye-SWCNT complex.[70] The conventional method for producing TiO_2/CNT composite for the DSSC involves a high temperature sintering at 450 °C. The high temperature sintering aids in the removal of the polymer and establishes a good interconnect between the TiO_2 particles. However in order to make flexible solar cells on the plastic substrates low temperature fabrication is required. *Lee et al* reported a low temperature fabrication process to form TiO_2/MWCNT photo anode and reported an efficiency of about 5.65%.[71] It is being observed that as the concentration of CNTs increases in the CNT/TiO_2 composite, the performance of the cell decreases due to the aggregation of the CNTs. Thus in order to improve the dispersion of the CNTs without causing damage to the side walls and the tip of the CNTs, Zhang et al. introduced oxygen containing groups on the surface of the CNTs by radio frequency inductively-coupled oxygen plasma treatment. The oxygen groups on the surface of the plasma treated CNT makes it hydrophilic and thus improves the dispersion. The Figure 8 compares the dispersion of TiO_2 between chemically modified CNT and plasma-treated CNT. The good dispersion of the TiO_2 leads to high surface area which in turn improves the dye loading and hence the overall efficiency. They have also shown that the addition of the plasma treated CNT brings about 75% enhancements in the efficiency.[72]

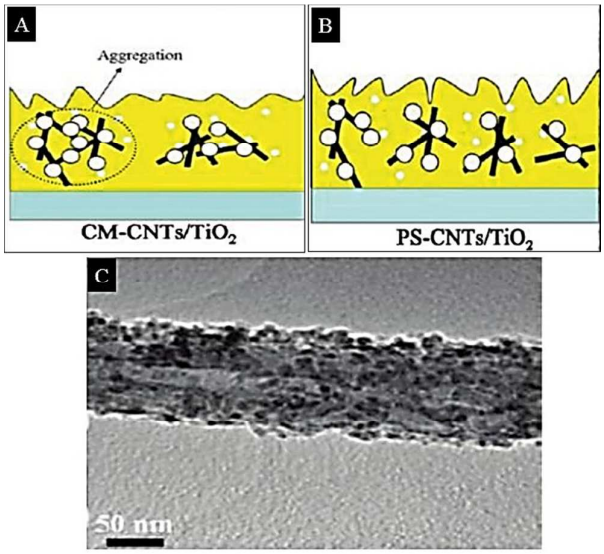

Fig. 8. Schematic showing the dispersion when chemically modified CNT (A) and plasma treated CNT (B) and (C) TEM image of plasma treated CNT/TiO_2 composite.[72]

Yun et al. synthesized TiO_2 hollow sphere/CNT composite by direct mechanical mixing and have shown an overall conversion efficiency of 4.71% with 0.1 wt.% of CNT. The enhancement in the efficiency is mainly due to the high surface area and hierarchical nanoporous structure. The Figure 9 shows the mechanism for the electron transport in TiO_2 hollow sphere/CNT composite.[73]

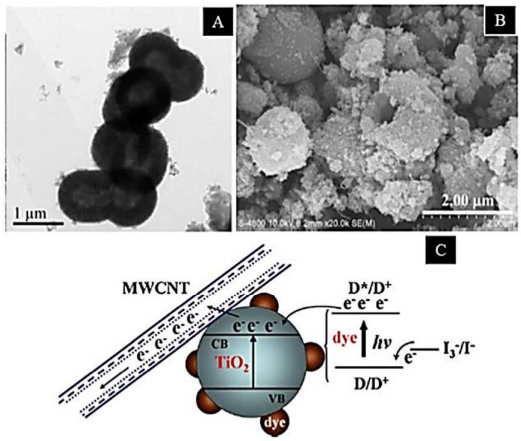

Fig. 9.A. TEM image of hollow spheres of anatase TiO_2, B. SEM image of TiO_2 hollow sphere/CNT composite and C. Schematic showing electron transfer mechanism in TiO_2 hollow sphere/CNT composite.[73]

Muduli et al. employed a hydrothermal route for the synthesis of TiO_2/MW-CNT composite, as the auto generated pressure upon heating aids in achieving crystalline phase with fewer defects at relatively lower temperature and have shown an enhancement in the power conversion efficiency of about 50% than the one without the MW-CNTs. The Figure 10B shows the functionalization of the CNT upon the hydrothermal treatment and bonding with the TiO_2 surface by ester bonds.[74]

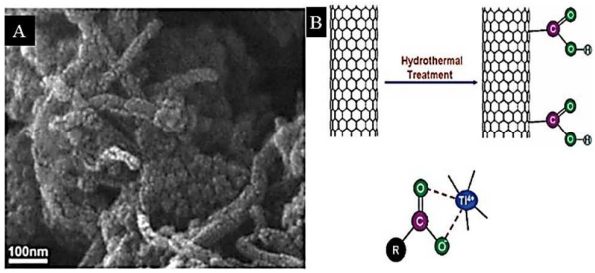

Fig. 10.A.SEM image of MW-CNT/TiO_2 composite and B. Functionalisation of CNT upon hydrothermal treatment. [74]

Dan et al. have succeeded in reporting a power conversion efficiency of 10.6% by using genetically engineered M13 virus as a template for the synthesis of single walled carbon nanotube-TiO_2 nanocrystal core-shell nanocomposite. The as-produced carbon nanotubes are generally a mixture of semiconducting and metallic forms. The semiconducting CNTs have a non-continuous band structure so that the electrons in the conduction band of the CNTs are easily transferred to the FTO thereby increasing the electron collection efficiency. However due to the continuous band structure of the metallic CNTs, the electrons transferred from the conduction band of the TiO_2 stays at the energy levels near the Fermi level thereby undergoing recombination with the dye and the electrolyte and thus reducing the overall energy conversion efficiency. M13 is a filamentous bacteriophage that can be genetically engineered to bind to the specific peptides. The Figure 11 shows the synthesis procedure of TiO_2/SWCNT complex with M13 virus as the template. The major advantage of this approach is that the M13 virus acts as a surfactant there by preventing the bundling of SWCNTs.[75]

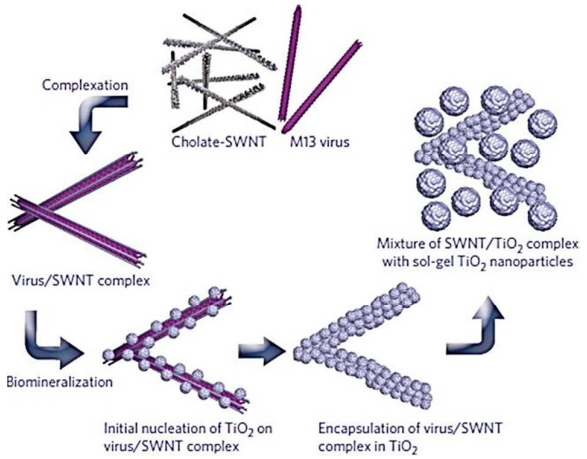

Fig. 11. The synthesis procedure of TiO_2/SWCNT complex with M13 virus as the template [75].

Subha et al. have successfully grown single-crystalline one dimensional rutile TiO_2 nanorods along with MWCNT on the FTO substrate by adopting a template-free synthesis method. They have also shown that the formation of TiO_2 and the anchoring of the same with that of the MWCNT have taken place simultaneously due to the presence of the polar oxygenated group. The composite used as photoanode in DSSC exhibited about 60% enhancement in the conversion efficiency.

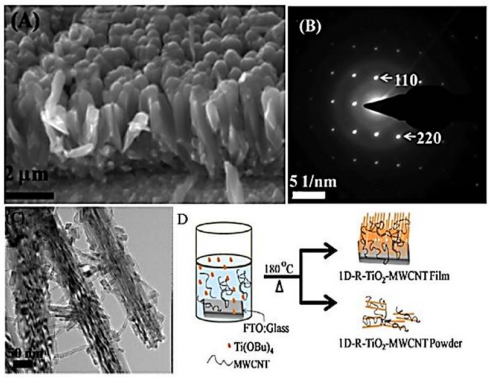

Fig. 12.A. SEM image B.SAED pattern C. TEM image of 1D- Rutile TiO_2 MWCNT composite grown on FTO.[76]

Since the TiO_2 nanowires are single crystalline, the grain boundaries are absent and hence the recombination reactions are prevented by providing a smooth electron transport path. The presence of MWCNTs facilitates better charge separation thus preventing the exciton recombination reactions.[76] Chang et al. employed a simple and facile electrophoretic deposition (EPD) technique. The DSSC fabricated using TiO_2 modified MWCNT as photoanode with natural dye extracted from Ipomoea showed about 30% enhancement in the power conversion efficiency with 0.01 g on CNT.[77] Patrick et al. electrophoretically deposited carbon nanotubes on the optical transparent electrode (OTE) followed by immersing the OTE into the TiO_2 colloid. The Figure 13A shows the schematic comparing the flow of electrons in the 1D TiO_2 nanostructures and CNT modified TiO_2 composite photoanodes in DSSC. The SWCNT facilitates better charge separation by preventing the electron back-transfer reaction. *i.e.* the recombination of the injected electrons with the oxidized dye thus improving the charge collection efficiency and have shown 45% enhancement in the short-circuit current density.[78]

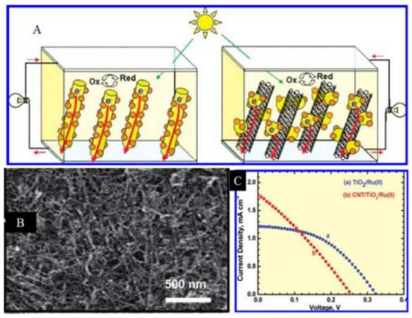

Fig. 13.A. schematic of electron flow in one dimensional nano structures and CNT modified TiO_2 photo anode. B. SEM image of the composite. C. J-V characteristics.[78]

Rice grain-shaped TiO_2/MWCNT was synthesized by Zhu et al. by the electrospinning method. The single crystallinity and the

high surface area of the composite had brought about a 32% enhancement in the energy conversion efficiency with 0.2 wt.% of CNTs.[79]

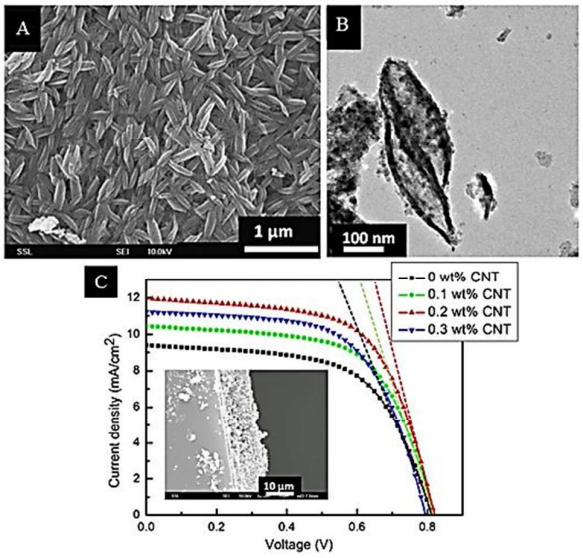

Fig. 14.A. SEM image B. TEM image and C. J-V characteristics of Rice grain shaped TiO_2-MWCNT composite.[79]

Zhang et al. synthesized flexible single wired DSSC by wrapping freestanding carbon nanotubes films around the co-axial Ti-TiO_2 nanotube wires. TiO_2 nanotube arrays radially anchored on Ti surface was synthesized by anodic oxidation and the same was wrapped by the free standing CNT by chemical vapour deposition. The DSSCs made with this material exhibit high stability and flexibility even at the bending angles up to 90°. The efficiency reported was about 1.6% which was further improved by an additional second conventional metal wire such as silver and copper.[80]

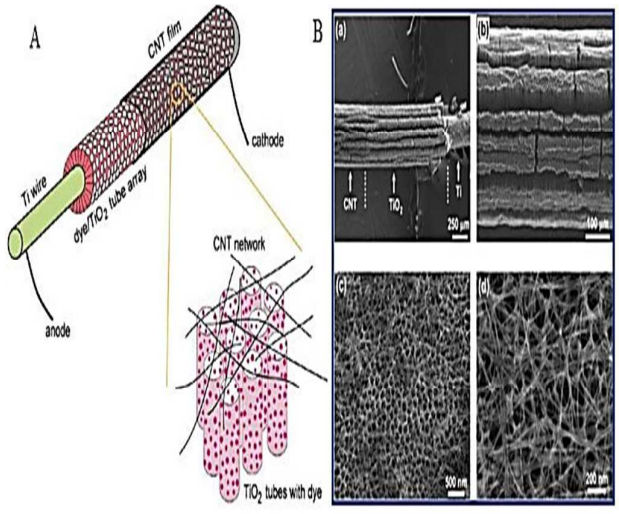

Fig. 15. Single wire DSSC wrapped by Carbon nanotube film electrode.[80]

COMPOSITE	METHOD	EFFICIENCY
MWCNT/TiO_2[68]	Direct mixing	10.29%
MWCNT/TiO_2[69]	MWCNT by thermal CVD and TiO_2 by Sol-gel	4.97%
CNT/TiO_2[72]	Plasma treated CNT	6.34%
CNT/TiO_2 hollow sphere[73]	Direct mixing	4.71%
MWCNT/TiO_2[74]	hydrothermal	7.37%
CNT/TiO_2[75]	Virus mediated method	10.6%
MWCNT/rutile TiO_2 nanorod[76]	Template free synthesis	2.4%
MWCNT/TiO_2[77]	EPD	0.35%
Rice grain shaped TiO_2/MWCNT[79]	electrospinning	6.12%
CNT film around co-axial Ti-TiO_2 nanotube[80]	Anodic oxidation of TiO_2 followed by CVD of CNT	1.65%

Table. 2. Summary of various CNT/TiO_2 composites, their synthesis procedure and photovoltaic performances.

GRAPHENE/TiO_2 COMPOSITES

The two-dimensional graphene sheets have high surface area and exhibit higher electrical conductivity than the one-dimensional carbon nanotubes. The higher electrical conductivity aids in faster electron transport and thus lowers the recombination. Due to single molecular layered structure graphene exhibits intermolecular forces such as physisorption and charge transfer interaction between graphene and TiO_2.[81] Thus the TiO_2 nanoparticles could anchor better on graphene so that the photo-induced electrons could be easily captured and transferred to the FTO. The Figure 16 shows the distribution of TiO_2 on the CNT and graphene. Yang et al. have compared the photovoltaic performance of CNT/TiO_2 and graphene/TiO_2 composite for DSSCs. The Electrochemical impedance spectroscopy studies reveal that the charge transfer resistance (R_{CT}=21.66Ω) is smaller for graphene/TiO_2 photoelectrode than that of the CNT/TiO_2 in which R_{CT} comes out to be 140 Ω. This result implies that the graphene/TiO_2 composite have higher electron transport rate than that of the CNT/TiO_2 composite.[82]

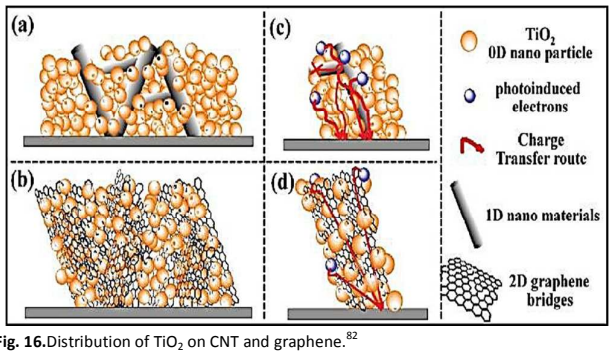

Fig. 16. Distribution of TiO_2 on CNT and graphene.[82]

The figure 17 shows the energy level diagram of DSSC when carbon nanostructures are added with TiO_2.

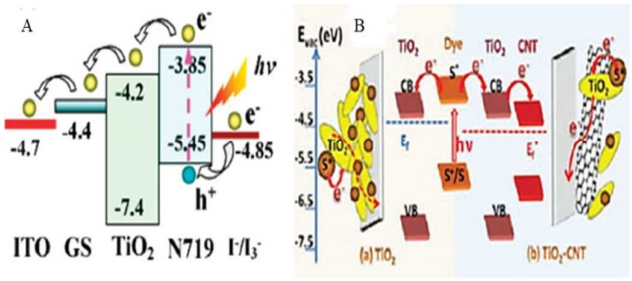

Fig. 17. Energy level diagram of DSSC when A. Graphene sheets are added [84] and B. CNTs are added.[79]

There are different ways by which TiO_2/graphene composites could be made. In general there are three important steps involved. They are: 1) mixing of graphene oxide with TiO_2, 2) reduction of graphene oxide to graphene by chemical reductants or UV radiation, 3) coating the composite on FTO followed by calcination at 450 °C.[83] However the major disadvantage is the aggregation of graphene and the poor contact with the metal oxide. Further dense and uniform distribution of the metal oxide is essential to promote electron transfer. Tang et al. proposed a method for incorporating graphene in nanostructured TiO_2 film by molecular grafting. The schematic (Figure 18) shows the incorporation of graphene sheets in nanostructured TiO_2 films by molecular grafting method. The conductivity of the reduced graphene sheets and good attachment of the TiO_2 could be achieved by controlling the oxidation time of the chemical exfoliation process. The graphene implanted TiO_2 showed conversion efficiency of 1.68%.[84] Zhou et al. developed a novel *in-situ* simultaneous reduction hydrolysis technique in ethylenediamine solvent. This method is based on simultaneous reduction of graphene oxide to graphene by ethylenediamine and formation of TiO_2 by the hydrolysis of titanium (IV) dihydroxybis and it is subsequently loaded *in-situ* onto graphene by forming Ti-O-C bonds. The DSSC fabricated using this composite showed a conversion efficiency of 7.1%.[85]

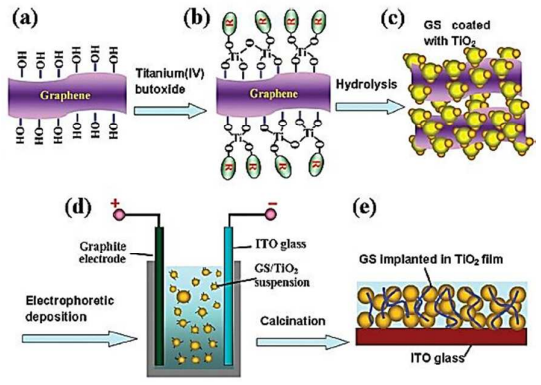

Fig. 18. Schematic of the molecular drafting method. [84]

A few layer graphene/TiO_2 nanocrystals were synthesized *in-situ* at a low temperature of 400 °C using $C_{28}H_{16}Br_2$ as a precursor and the composite was used in DSSC as photoanode by Liu et al. During the *in-situ* thermal decomposition processes, both C-doped TiO_2 and few-layer graphene (FLG) – TiO_2 composites were formed.

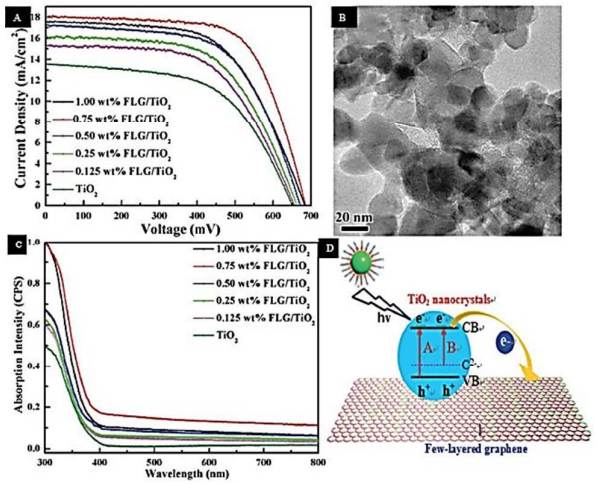

Fig. 19.A. J-V characteristics of graphene/TiO2 composite B. TEM image of graphene/TiO_2 composite C. Absorption spectra of graphene/TiO_2 composite and D. Schematic showing electron transfer mechanism.[86]

The optical absorption spectra showed an enhanced UV and visible light absorption for FLG-TiO_2 composite than the bare TiO_2 nanocrystal. They have reported that this enhancement in the absorption with the redshift is due to the formation of the C- doping. Under irradiation, the electrons can be excited from the valence band to the conduction band of the TiO_2 or from the carbon impurity level to the conduction band of TiO_2 as shown in the Figure 19D. Thus the optical absorption spectrum increases due to the band-gap narrowing. Further the charge transport is also enhanced having a short-circuit current density of 18.03 mA cm^{-2} and a photovoltaic conversion efficiency of 8.25% was reported for DSSC with 0.75 wt.% of few layer graphene.[86] Tsai et al. made graphene-TiO_2 composite by mixing TiO_2 powder with different wt.% of graphene and made DSSC by spin-coating it on the ITO substrate. They have shown that with a graphene content of about 1 wt.% in TiO_2 film, there is an improvement in efficiency from 5.98% to 6.86%[87]. The hydrothermal synthesis of TiO_2/graphene composites generally involves multiple steps.[88] Anjusree et al. reported one pot synthesis of TiO_2/graphene nanocomposites. According to their results, the average thickness of the graphene sheets was 1.1 nm and the TiO_2 nanoparticles were dispersed uniformly on the surface of the graphene sheets. The results are shown in the Figure 21. The DSSC made with the composite having 0.7 wt.% of graphene showed an efficiency of 4.26% which is 25% higher than the one without graphene.[89]

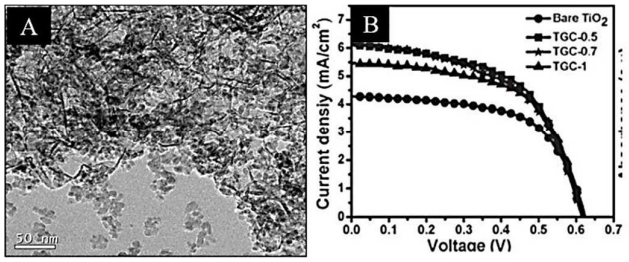

Fig. 20.A. TEM image of graphene/TiO_2 composite by one pot hydrothermal method and B. J-V characteristics.[89]

Graphene composited TiO_2 by one-step solvothermal process was reported by Ziming et al. They synthesized graphene/TiO_2 composites with different TiO_2 nanostructures like ultra-small 2 nm TiO_2 nanoparticles (USTG), 12 nm nanoparticles (STG) and nanorods (NRTG) just by controlling the solvothermal reaction conditions. The Figure 21 shows the schematic of producing graphene/TiO_2 composites. Among the three different nanocomposites, the composite with ultra-small 2 nm TiO_2 particles showed the modest efficiency of 7.25%. The high efficiency is attributed to high specific surface area produced by ultra-small TiO_2 nanoparticles and the lower recombination rate.[90] Reduced graphene oxide/TiO_2 nanocrystal composite was prepared by Shu et al. by solvothermal method and they are used as photoanodes in DSSC. The DSSC with 0.75 wt% of r-GO showed maximum power conversion efficiency of 5.5% which is about 35% higher than the DSSC with the conventional P25.[91] Hierarchical titania mesoporous sphere/graphene composite was synthesized by controlled hydrolysis of titanium precursor in the presence of graphene oxide followed by the hydrothermal treatment. The high surface area of both graphene and mesoporous sphere increases the dye absorption and the high electrical conductivity of graphene improves the charge transfer and collection efficiency. The DSSC constructed using this composite as photoanode showed 7.19% cell efficiency.[92]

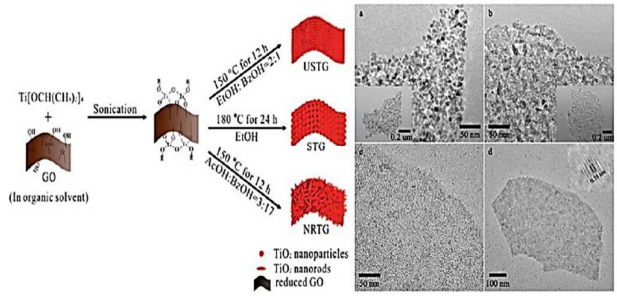

Fig. 21. Schematic showing the solvothermal synthesis and the TEM images of (a) STG (b) NRTG (c) USTG high magnification (d) USTG low magnification. [90]

Sun et al. reported a simplest method for making graphene/TiO_2 composite by heterogeneous coagulation. It is based on the principle that when two types of particles with opposite charges are mixed together, mutual coagulation occurs. The graphene used in their work was nafion functionalized. The hydrophobic interactions of the fluro backbones of nafion prevent graphene aggregation. The overall energy conversion efficiency comes out to be 4.28%.[93] Asha et al. reported a simple and cost-effective method to form graphene/TiO_2 composite. Molten salt synthesis is a technique by which nanoparticles with varied morphology could be made.[94] In this method graphene was added to TiO_2 at the early stage of the growth of the TiO_2 from its precursor solution thus ensuring uniform distribution of graphene on the TiO_2 matrix. The graphene forms a bridging layer between the TiO_2 networks. The overall energy conversion efficiency comes out to be 5.41%.[95]

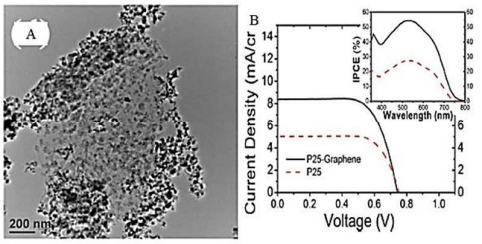

Fig. 22.A. TEM image of Nafion functionalised graphene/P25 composite and B. J-V Characteristics[93].

Compared to the zero-dimensional nanostructures, one-dimensional nanostructures provide a direct pathway for the electrons to travel thereby by reducing the loss of the electrons by recombination.[96] The one-dimensional nanostructures also act as light scattering centres scattering light in the red part of the spectrum thereby increasing the light absorption by the dye molecules[97] and thus enhance the light harvesting efficiency. Thus the preferred morphology of the TiO_2 for better electron transport and improved light scattering is the one-dimensional structures. Electrospinning is one of the most common ways for producing one-dimensional nanostructures such as nanowires, nanofibers and nanorods. Zhu et al. synthesized one dimensional TiO_2/graphene composite using CTAB functionalized graphene mixed with the polyvinyl pyrrolidone (PVP) polymer as the electrospinning solution and reported 6.49% of cell efficiency.[98] Conductive nanofiber mats were synthesized by electrospinning TiO_2/graphene composite using PVP as the carrier solution by Asha et al. The DSSC assembled using this nano fiber mat as photoanode showed efficiency of 7.6%.[99] The Figure 23C shows the TEM image of the electrospun TiO_2/graphene composite. Wang et al. fabricated graphene sheets on highly oriented TiO_2 nanotube arrays by one-step electrochemical method. The surface coverage of the nanotube arrays by graphene was controlled by controlling the reaction time and they have reported a photovoltaic conversion efficiency of 4.46%.[100] However the smooth-walled TiO_2 nanotubes have a very low internal surface area and as a result the dye loading is poor which in turn reduces the light harvesting efficiency and the overall efficiency of the cell. So the surface area must be improved without compromising the one-dimensional architecture. The surface area of the nanotube arrays were improved by ridges on the surface of the nanotube thus forming bamboo-type TiO_2 nanotubes.[101-102] Luan et al.

electrophoretically deposited reduced graphene oxide on the bamboo-type TiO_2 nanotube array and they reported an efficiency of about 6.01%.[103]

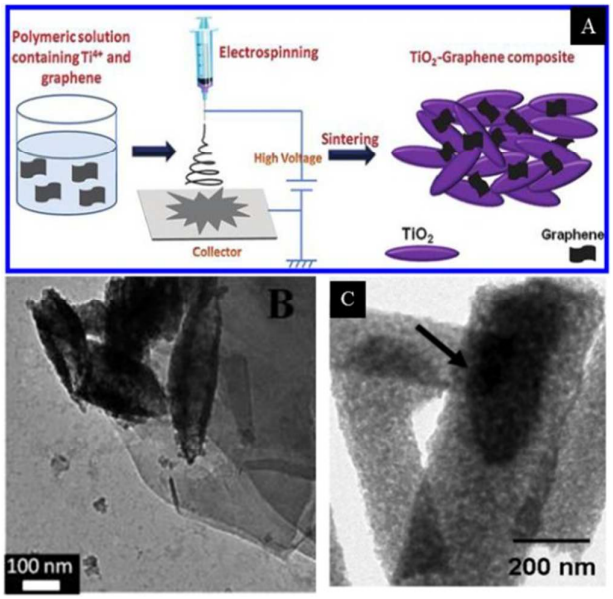

Fig. 23.A. Schematic of electrospinning.[98] B. Rice grain shaped TiO2/graphene composite. [98] C. graphene/TiO_2 by electrospinning.[99]

In comparison with the one-dimensional nanostructures, two-dimensional nanostructures have a very high surface area and they are mostly employed as scattering layers in DSSC. However the photoanodes made of two-dimensional nanosheets show inferior performance than that of one-dimensional nanostructures due to the poor conductivity of the TiO_2 films and inferior contact between the FTO and the TiO_2 film.[104] So in order to overcome this demerit, Fan et al. fabricated a two-dimensional TiO_2 nanosheets/graphene composite films and fabricated DSSC which showed photovoltaic conversion efficiency of 5.77%. They attributed that the improvement in the efficiency is due to the following reasons: 1) good anchoring between TiO_2 nanosheets and the two-dimensional graphene sheets, 2) the two-dimensional structures provide a very high surface area thereby more sites for the loading of dye molecules, and 3) due to the large pore volume, the electrolyte diffusion is enhanced and as a result the dye is regenerated faster.[105] In addition to 0-D TiO_2/graphene composites, 1-D TiO_2/graphene composites and 2-D TiO_2/graphene composites, composite with graphene containing both zero and one dimensional TiO_2 nanostructures were used as bilayer photoanodes in DSSC. TiO_2 nanotubes are adhered onto the FTO coated with graphene/TiO_2 nanoparticles. The 1-D nanotube causes the scattering of light and the 0-D nanoparticles provide a very high surface for good dye loading thus improving the light harvesting. Further, graphene aids in the hassle-free transport for the electrons and the overall energy conversion efficiency comes out to be 6.29% with 0.1 wt.% of graphene.[106]

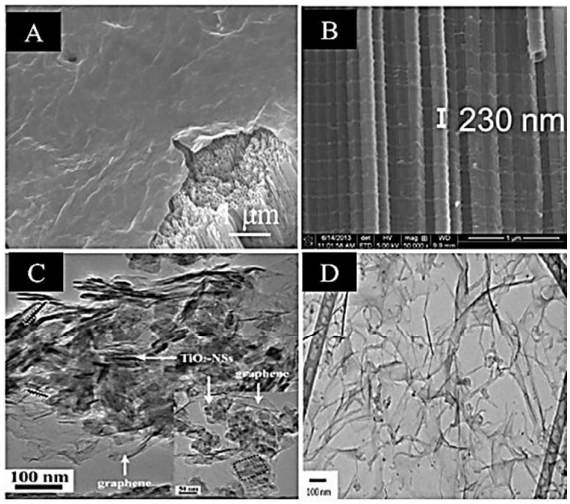

Fig. 24.SEM image of A. graphene oxide on TiO_2 nanotube arrays[100] and B. Bamboo type TiO_2[103] .Tem image of C. TiO_2 sheet/graphene composite [105] and D. MWCNT/Graphene/TiO_2 hybrid [108].

Tang et al. reported a three-layered photoanode in which alternating graphene/TiO_2 acts as the electron transport layer, P25 as the working layer and graphene/titanate nanotubes as the scattering layer. The graphene/TiO_2 composite was synthesized by layer-by-layer self-assemble technology and the graphene/titanate nanotubes were synthesized by the hydrothermal route. The superior light scattering and the electron transport properties of the composite film were responsible for the overall conversion efficiency as high as 8.67%.[107] The high specific surface area and strong π-π interactions between the graphene sheets prevent the dispersion of graphene. Yen et al. introduced MWCNTs on the graphene which reduces the π-π interactions thereby reducing the aggregation. An optimum ratio of about 2:1 of MWCNT to graphene aids in the better dispersion and have achieved an overall conversion efficiency of 6.11%.[108]

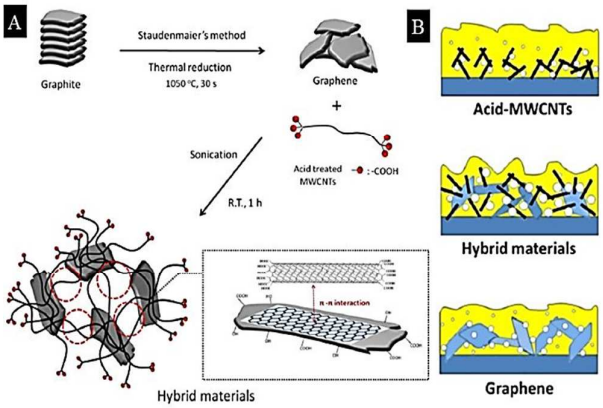

Fig. 25. Schematic showing the synthesis of MWCNT/Graphene/TiO_2 hybrid material[108].

Graphene-coated TiO_2 core-shell structure was synthesized and its photocatalytic and the photoelectrical properties were studied by Kim et al. The enhanced H_2 production and the

photocurrent generation of graphene shell coated TiO_2 than that of the typical TiO_2 coated graphene sheets proves it to be a promising architecture for solar energy conversion.[109]

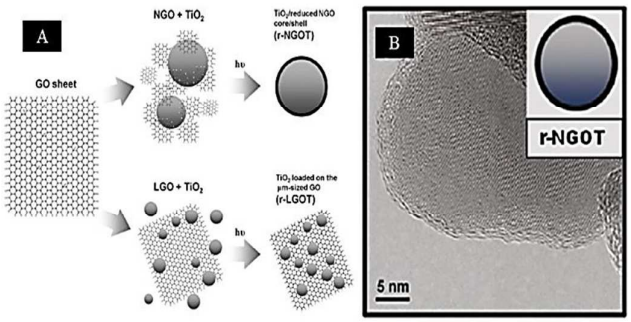

Fig. 26.A. Synthesis procedure of TiO_2/graphene core shell B. TEM image of TiO_2/graphene. [109]

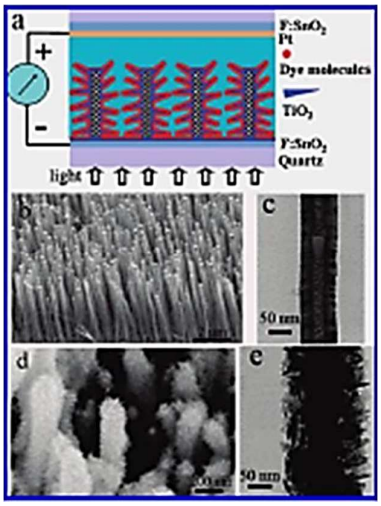

Fig. 27.TiO_2 coated vertically aligned carbon nanofibers.[112]

In addition to carbon nanotubes and graphene, carbon nanofibers also aid in the facile transport of electrons through the TiO_2 film. One such hybrid composite was reported by Liu et al. in which vertically aligned CNFs were grown by plasma enhanced chemical vapour deposition (PECVD) and the same was coated with TiO_2 needle-like structures by metal-organic chemical vapour deposition (MOCVD) forming a co-axial nanowire array structure. They have achieved an overall low power conversion efficiency of about 1.09%.[112]

ROLE OF GRAPHENE QUANTUM DOTS

In order to develop a low cost and eco-friendly DSSC with the reduced use of Ruthenium dye containing heavy metal like ruthenium, graphene quantum dots-optimized photoanodes were reported by Fan et al. The short-circuit current density and the power conversion efficiency of the DSSC with quantum dot optimized photoanode was 30.9% and 19.6%? higher than that of the conventional DSSC, respectively. The photo-excitation of graphene quantum dots and the hot electron injection quantum dots to TiO_2 were responsible for the outstanding performance inspite of the minimum dye loading.[110]

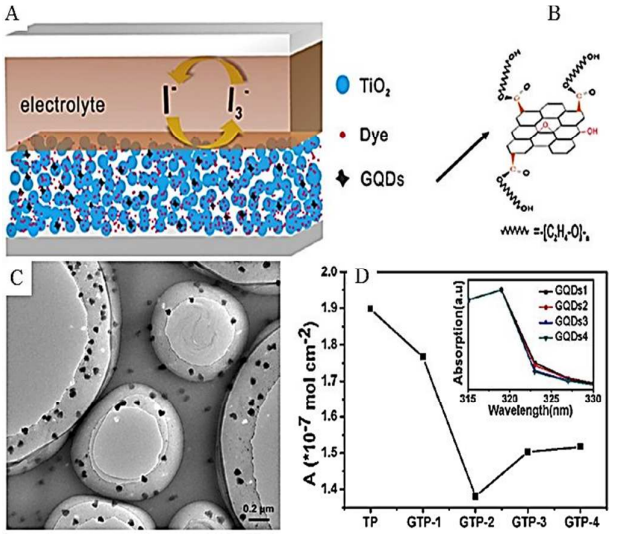

Fig. 28.A. Structure of graphene quantum dot modified solar cell. B. Structure of graphene quantum dot. C. SEM image of graphene quantum dot. D. Amount of dye loaded.[110]

Lee et al. successfully fabricated highly luminescent graphene quantum dots by oxidation of herring bone type carbon nanofibers followed by size selective precipitation. The size-selective precipitation helps in the separation of the nanometer-sized quantum dots from the bulk graphene quantum dot solution. These graphene quantum dots exhibited up-conversion PL properties and the DSSC with 2.6 mg of graphene quantum dots showed 9.2% enhancement in the power conversion efficiency than the pristine DSSC.[111]

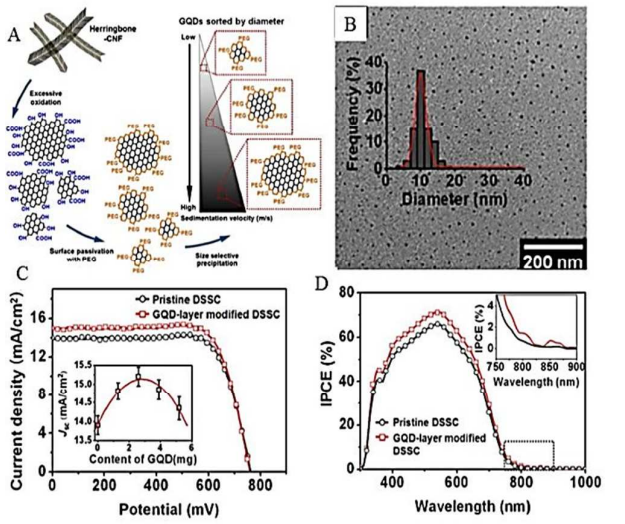

Fig. 29.A. Synthesis procedure of graphene quantum dot (GQD), B. TEM image of GQD, C. J-V Characteristics and D. IPCE measurement .[111]

COMPOSITE	METHOD	EFFICIENCY
Graphene/TiO_2 [84]	Molecular grafting	1.68%
Graphene/TiO_2 [85]	Simultaneous reduction hydrolysis	7.1%
Graphene/TiO_2 [89]	hydrothermal	4.26%
Ultra small TiO_2 nanoparticle/graphene [90]	solvothermal	7.25%
r-GO/TiO_2 [91]	solvothermal	5.5%
Mesoporous titania/graphene [92]	hydrothermal	7.19%
Graphene/TiO_2 [93]	Heterogeneous coagulation	4.28%
Graphene/TiO_2 [94]	Molten salt	5.41%
Graphene/TiO_2 [99]	electrospinning	7.6%
rGO/Bamboo type TiO_2 nanotube array [103]	Electrophoretic deposition	6.01%
TiO_2 sheet/graphene [105]	Hydrothermal	5.77%
Vertically grown CNF/TiO_2 composite [112]	MOCVD deposition of TiO_2 on PECVD grown CNF	1.09%
Rice grain shaped TiO_2/graphene [98]	electrospinning	6.49%
Graphene/TiO_2 [87]	Spin coating	6.86%

Table 3 Summary of various graphene/TiO_2 composites, their synthesis procedure and photovoltaic performances.

ROLE OF CARBON NANOSTRUCTURES AT TiO_2/FTO INTERFACE

The carbon nanostructures not only enhance the electron transport through the TiO_2 network but also increase the electron collection efficiency by minimizing the interfacial resistance at the TiO_2/FTO interface.

In addition, the recombination reactions at the TiO_2/dye/electrolyte and TiO_2/TiO_2 interfaces, the possible centre for recombination are the TiO_2/FTO interface. In order to prevent the recombination at the TiO_2/FTO interface, conventionally the FTO is subjected to a pre-treatment by hydrolysing it with $TiCl_4$ forming a thin layer of TiO_2.[113] However since $TiCl_4$ hydrolyses faster when exposed to air, there is a need for an alternative to be used as an electron transporting layer at TiO_2/FTO interface without compromising the transmittance of the FTO. Chen et al.'s was the first group to report on the functionalization of FTO using graphene as the electron transport layer at the TiO_2/FTO interface. The graphene was deposited on FTO by spin-coating. Since the work function of graphene lies below than that of the TiO_2, and also matches with that of the FTO, the electron transport from graphene to TiO_2 is prevented. Thus the interface functionalization leads to 8% enhancement in the power conversion efficiency than the one pre -treated with $TiCl_4$.[114] Hu et al. deposited 60 nm thin layer of graphene on ITO by sputtering. The graphene prevents the back reaction and thus the short-circuit current density and the power conversion efficiency increases from 6.9 mA/cm^2 and 1.45% to 17.5 mA/cm^2 and 3.98%, respectively.[115] Photocatalytically reduced mixture of graphene oxide/TiO_2 mixture was introduced as the interfacial layer at the FTO/TiO_2 interface by Kim et al. and the power conversion efficiency was improved from 4.89% to 5.26%.[116]

ROLE OF CARBON NANOSTRUCTURES IN THE COUNTER ELECTRODES

The other important component in the DSSC is the counter electrode. The counter electrode acts as a catalyst to reduce the I^-/I_3^- redox couple electrolyte. The redox reaction usually takes place at the electrode/electrolyte interface. The reaction is given as:

$$I_3^- + 2e^- \Leftrightarrow 3I^-$$

The most commonly used counter electrode is the platinum due to its outstanding chemical and electrochemical stability, low charge transfer resistance and higher catalytic activity towards I^-/I_3^- redox species. However inspite of all these merits, high cost, less availability and the degradation of the counter electrode due to the electrolyte and the catalyst forming PtI_4,[117] there is a need for an alternative conductive counter electrode material. Further the highly corrosive nature of the electrolyte restricts the use of other metals such as silver aluminium, copper, nickel and gold as counter electrodes.[118] These requirements opened up the way for carbon materials-based counter electrodes due to good electrical conductivity, resistance against corrosion and catalytic reduction of the redox couple.[119-120]

1. CARBON BLACK AND ACTIVATED CARBON

The catalytically active sites in carbon materials are mostly located at the crystal edges. As a result carbon materials with low crystallinity and edges are considered to be catalytically more active than the highly oriented CNT and graphene. One such carbon material with low crystallinity is carbon black.[121] It is mostly produced by incomplete combustion of heavy petroleum products, coal tar and vegetable oil. The first carbon-based counter electrode was developed by Kay and Gräztel in 1996 making use of 20% carbon black, 15% nanocrystalline TiO_2 added to graphite powder. The enhanced the catalytic activity was due to the high surface area carbon black.[118] In addition, the photovoltaic parameters such as fill-factor and efficiency were found to be dependent on the thickness (roughness factor) of the film. As the thickness (roughness factor) is increased, the fill-factor also increases due to the apparent decrease in the charge transfer resistance

for the redox reaction of I^-/I_3^- redox couple.[121-122] However, the catalytic activity of carbon-based counter electrodes is comparable with that of platinum only if the thickness is greater than that of few tens of micrometer.[122] This not only reduces the transparency but also increases the internal resistance leading to the reduction in the efficiency. Thus nanocarbon powders with average particle size of 30 nm and a surface area of 100 m^2/g was used as a counter electrode and the performance was compared with that of microcarbon-based counter electrode. The DSSC with nanocarbon based counter electrode showed an efficiency of 6.73%.[123] Pure carbon-based flexible counter electrode for DSSCs was fabricated by Chen et al. using graphite sheet as a substrate and 20 µm thick activated carbon as the catalytic layer. The reduction of the sheet resistance increases the fill-factor as well as the overall energy conversion efficiency of the cell. The fill-factor and efficiency of pure carbon based counter electrode comes out to be 70.2 and 6.46%, respectively.[124]

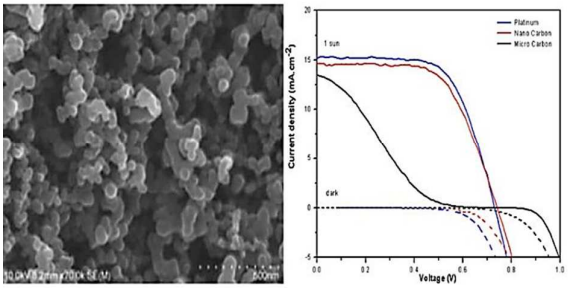

Fig. 30.SEM image of Nano carbon and J-V characteristics of DSSC comparing Nano carbon and micro carbon[123].

2. MESOPOROUS CARBON

The mesoporous carbon materials have very large internal surface area and narrow pore size distribution. Mesoporous carbon material prepared by the self-organization of the surfactant and the carbon precursor was used as counter electrode in DSSC and the performance was compared with that of the activated carbon by Wang et al. and they have shown that the DSSC with mesoporous carbon as the counter electrode showed better performance than the one with activated carbon mainly due to the difference in the pore size distribution of the mesoporous and the activated carbons. The easily accessible pore size of the mesoporous carbon aids in better ionic diffusion and thus improves the fill-factor and the overall cell performance.[125] According to EIS studies, counter electrodes based on electrospun carbon nanofibers also proves to a low-cost alternative due to low charge transfer resistance, large capacitance and high reaction rate for the tri-iodide reduction. However, the overall performance was not comparable with that of the Pt. counter electrode due to lower fill-factor which could be substantially improved by using thinner and porous carbon nanofibers.[126]

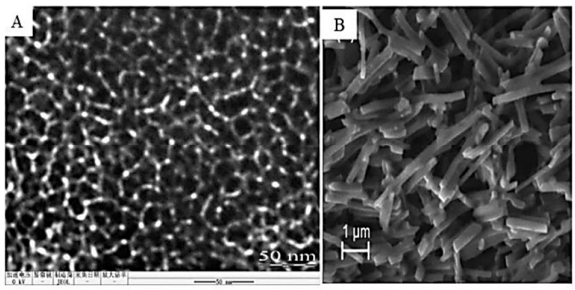

Fig. 31.A) TEM image of mesoporous carbon [125] and B) SEM image of electrospun carbon nanofiber on FTO.[126]

3. INVERSE OPAL CARBON

The inverse opal carbon is a 3-D structure with interconnected pores which aids in both fast electron transport and diffusion of the electrolyte ions. Three different types of inverse opal carbon-based counter electrodes namely inverse opal carbon, inverse opal carbon with mesopores and graphitized inverse opal carbon were fabricated by Kang et al. The inverse opal carbon with the mesopores showed better performance than the other two forms due to higher specific surface area and the interconnected ordered pores. The DSSC showed an overall energy conversion efficiency of 5.5% which is comparable with that of platinum which comes out to be 5.8%.[127]

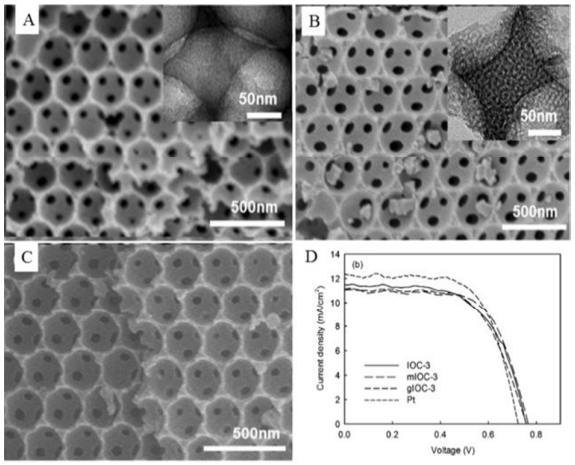

Fig. 32.SEM images of A) inverse opal carbon, B) inverse opal carbon with mesopores, C) graphitized inverse opal carbon, D) J-V Characteristics.[127]

4. HIERARCHICAL CARBON NANOSTRUCTURES

Hierarchical nanostructured carbon counter electrode with 60 nm diameter hollow macroporous core and 30 nm thick shell with large surface area and mesoporous volume showed an energy conversion efficiency of 7.56% and fill-factor of 67% which is comparable with that of the Pt-based counter electrode. The unique feature of this hierarchical structure is that the macroporous hollow core acts as an electrolyte buffering reservoir, thus reducing the diffusion distance to the interior surface of the shell. Further the 3D large inter-connected interstitial volume favours fast transfer of electrons

and ions. Thus both the porosity and the hierarchical nanostructure are responsible for efficient mass transport and the enhancement of the performance of the performance of the cell.[128] A hierarchical porous carbon structure with a lot of micropores generated within the walls of the mesoporous carbon was synthesized by Wang et al. by a combination of self-assembly and chemical activation method. The highest surface area of about 1661 m^2/g enhances the electrocatalytic activity and the overall conversion efficiency was 6.48% similar to that of the Pt counter electrode.[129] Electrospun-activated carbon nanofibers with a hollow core and a highly mesoporous surface with a mesoporous surface area of 151 m^2g^{-1} used as counter electrode in DSSC showed an efficiency of 7.21%. The hollow core - mesoporous shell structure facilitates better electron and ion exchange by increasing the contact area between the fibres and the electrolyte. This in turn promotes the I_3^-/I^- redox reduction reaction. In addition, the 1-D morphology facilitates directional electron transport. Thus the synergetic effect of both the one dimensional structure and the higher catalytic activity were responsible for the improvement in the overall cell performance[130a]. Pt nanoparticles are attached to the surface of the carbon nanofibers synthesized by electrospinning followed by stabilisation and carbonisation and subsequent growth of Pt nanoparticle through redox reaction. The DSSC was fabricated with this composite as the counter electrode and the performance of the device was found to be dependent on the concentration of the Pt loading. The surface attached Pt nanoparticles on electrospun carbon nanofiber results in more number of catalytic active sites leading to higher electrocatalytic activity. This in turn lowers the charge transfer resistance. Maximum efficiency of 7.6% was obtained for the composite having 200wt% of Pt nanoparticles on the electrospun carbon nanofiber[130b]. carbon nanofiber/TiO2 nanoparticle composite as a counter electrode material was synthesized by Sigdel et al. the composite was deposired on the FTO by spray coating and the DSSC fabricated showed a power conversion efficiency of 7.25% under one sun illumination. The performance of the device was further improvrd by adding 8wt% of Pt to the composite[130c].

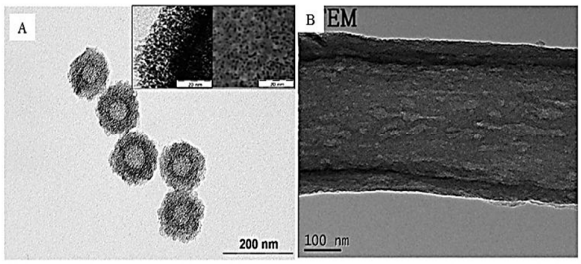

Fig. 33.TEM images of A) Hierarchical nanostructured carbon with hollow macropore [128], B) Electrospun activated carbon nanofiber.[130a]

5. SUB-MICROMETER SIZED GRAPHITE

Graphite is a conducing material that is available in abundance in nature. However when compared with the basal planes, the edge planes of the crystal exhibits faster electron transport.[131] Thus the edge plane proves to be catalytically more active than the basal planes. The sub-micrometer sized graphite with abundant edge planes enhances the reduction rate of I_3^-. The DSSC fabricated with 9 µm thick spin-coated graphite layer as counter electrode showed a photovoltaic conversion efficiency of 6.2%.[132]

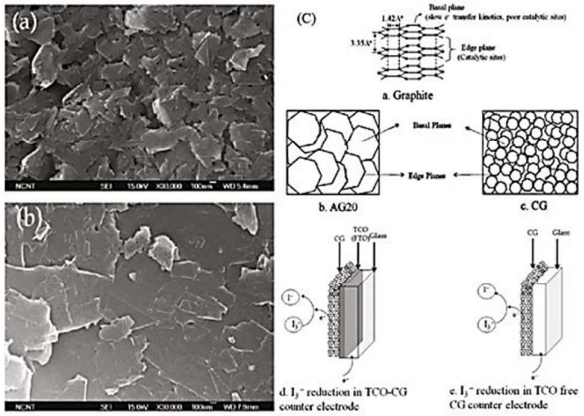

Fig. 34.SEM images of a) sub-micron sized graphite, b) micron sized graphite and c) Schematic of graphite and reaction at counter electrode.[132]

6. FULLERENES

Fullerenes, also called as Bucky balls, are an allotrope of carbon containing sp^2 hybridized carbon atoms resembling a soccer ball with twenty hexagons and twelve pentagons as the basis of an icosahedral symmetry closed cage structure.[133] Thin films of fullerene were deposited on ITO by a coating method called as electrolyte micelle disruption method using surfactants. The Figure 35 shows the schematic of the micelle disruption method. The thickness of the coating was controlled by controlling the electrolysis time and the highest efficiency was obtained for thin films formed by electrolysis for 2 h.[134]

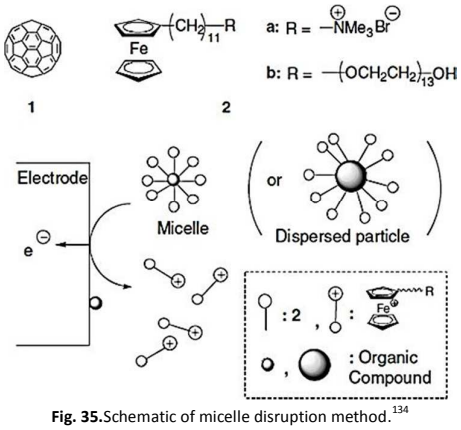

Fig. 35. Schematic of micelle disruption method.[134]

7. CARBON NANOTUBES

The carbon nanotubes have attracted greater attention due to the high surface area and electron transport properties. Suzuki et al. compared the performance of DSSC with SWCNT, carbon filaments (multiwalled carbon tubes with 1 µm diameter and

10-40 µm length) and nanohorns as counter electrode. The SWCNT with largest surface area of 764 m^2g^{-1} showed an efficiency of 4.5% due to the enhanced electrochemical catalytic activity. In addition, the good contact between the SWCNTs reduces the resistance and also increases the mechanical strength of the film.[135] Ramasamy et al. spray-coated multiwalled CNTs on the FTO and from the electrochemical impedance spectroscopy studies they have shown that the charge transfer resistance value of these counter electrodes decreases with the increase in the spraying time which eventually increases the photovoltaic parameters.[136] Although the CNTs exhibit good catalytic activity towards the tri-iodide reduction, the catalytic activity could be further enhanced significantly by introducing defect sites on to the CNTs. This could be done by exposing the CNTs to ozone. For an exposure time of about 20 minutes, the catalytic activity increases significantly without changing the light transmission or the sheet resistance. However, longer exposure of the CNTs to ozone removes the CNTs thus increasing the transmittance, R_{ct} as well as the sheet resistance.[137] However most of these carbon nanostructures were deposited as 2D films employing wet chemical approach which limits the catalytic activity. The vertically aligned SWCNT deposited on the FTO by a dry transfer approach is a simple and repeatable technique and it offers high density of SWCNT arrays. The device performance was found to be dependent on the length of the CNTs and the DSSC fabricated with an optimal length of 34 µm CNTs showed an overall power conversion efficiency of 5.5%.[138] When the graphene sheets were rolled in parallel with the tube axis, hollow-structured multiwalled CNTs were formed whereas when the graphene sheets were folded at an angle with the tube axis, bamboo-type multiwalled CNTs were formed.[139] Since the electron transfer kinetics in the edge planes are faster than the basal planes, the defect rich basal planes of the bamboo type CNTs facilitates faster electron transport and proves to be a suitable alternative for the platinum counter electrode. The constant R_{ct} value during the temporal evaluation has shown that the counter electrodes made of these MWCNTs are stable. The presence of the defect edge plane was proven by Raman spectroscopy with highly intense D bands. Inspite of the high V_{oc} and efficiency, the J_{sc} is poor because of the opaque nature of the MWCNT which restricts the reflection of the unabsorbed solar spectrum towards the TiO_2 photoanode.[140] In order to build DSSC with carbon nanotube based counter electrodes showing performance similar to that of the platinum-based counter electrodes retaining both high efficiency and the transparency at the same time, Cha et al. synthesized MWCNT microballs and deposited it on the ITO. The DSSC performance as well as the transparency can be tuned by controlling the deposition time. The DSSC with CNT microball-based counter electrode with 70% transparency can reach efficiency of about 80% of that of the platinum counter electrode.[141] The electrical and the electrochemical properties of the CNTs are dependent on the dispersion of the CNTs. If the CNTs aggregate together to form bundles, the surface area is reduced, which in turn alter the properties of CNTs. In order to fabricate DSSC with MWCNT with better dispersion, water soluble MWCNTs with covalently attached polyelectrolytes were synthesized by Han et al. using an electrostatic spray method. The Figure 37A shows the schematic of the synthesis using the grafting route. The photovoltaic conversion efficiency of the DSSC comes out to be 7.03%.[142]

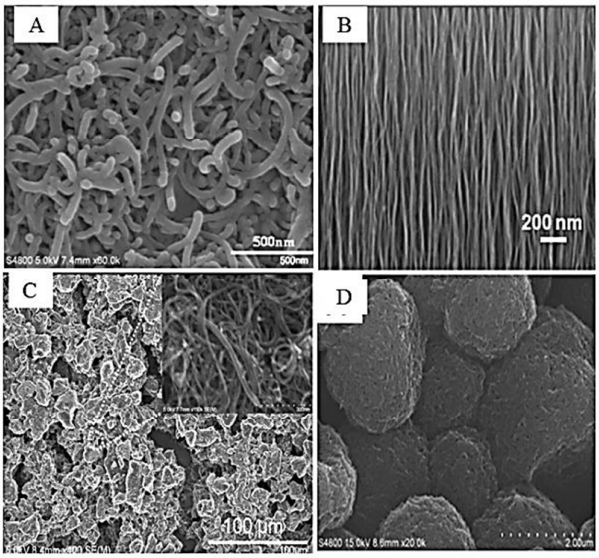

Fig. 36. SEM images of A) Multiwalled CNT[136], B) Vertically aligned SWCNT[138], C) Bamboo type MWCNT [140] and D) CNT microballs [141].

Free-standing flexible single walled carbon nanotube called as bucky papers treated with plasma had vertically oriented, micron-sized, pillar-like structure on its surface and the base with a dense mesh of single walled carbon nanotubes. The performance of the DSSC fabricated was comparable with that of platinum due to larger accessible surface area and enhanced catalytic activity.[143] In addition, composites of MWCNT with conductive polymers such as PEDOT:PSS were also being used as counter electrodes.[144a]

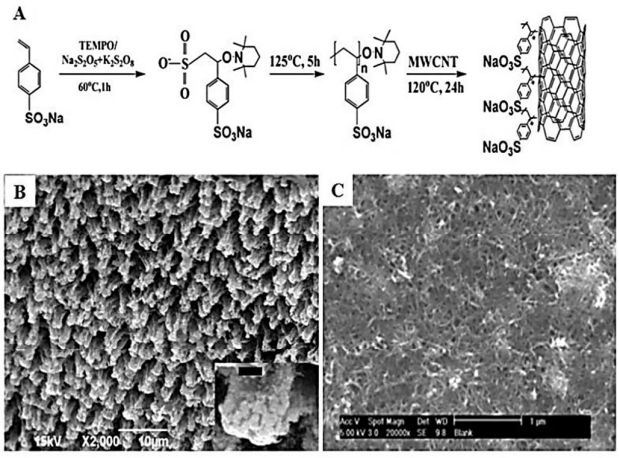

Fig. 37.A) Schematic of synthesis of water soluble MWCNT [142], B) SEM image of Bucky paper [142] and C) Conducting polymer/CNT composite. [144a]

ALIGNED CARBON NANOTUBES

In order to improve the applications of the carbon nanotubes, it becomes necessary to extend the properties of the CNTs from the nanoscale to the macroscopic scale which could be done by tuning the alignment of the CNTs Sun et al. have highlighted the various synthetic strategies, properties and applications of aligned CNTs.[144b] If the CNTs are randomly oriented with lots of inter connections, boundaries and contacting points, the charge separation and transport of the charges are hindered resulting in poor efficiency. Thus in order to overcome these hinderances, the fabrication of the aligned CNTs with highly oriented geometry becomes an effective solution. Making use of these aligned CNTs both planar and non- planar wire shaped flexible DSSC had been fabricated. Yang et al. synthesized aligned carbon nanotube sheets with good transparancy, flexibility and electrical conductivity as a counter electrode material and compared the photovoltaic performance of DSSC based on aligned CNT with that of DSSC based on randomly oriented CNT film. Firstly, CNT were prepared using CVD. These synthesized CNT were later spun using a blade. This was further transferred onto a FTO glass and poly (ethylene terephthalate) to check for its transparency7. Using this system they achieved a conversion of 4.18%. On the other hand, randomly arranged CNT gave an efficiency of 3.24%. the major reason for higher efficiency of the aligned CNT than the randomly arranged CNT is, as it is randomly arranged, the charge carriers have to cross over multiple points to reach the electrolyte which is not in case of aligned CNT. They have also shown that the structure and the electrical conductivities of the CNTs remain unchanged even after the deformable bending process.[144c] Lee et al. synthesized vertically aligned N- doped carbon nanotube arrays via growth detachment process. The doping of the CNT with electron rich nitrogen reduces the band gap of the CNT thus making it metallic which in turn resulted in high conductivity and catalytic activity. The fill factor and efficiency of the DSSC comes out to be 0.67 and 7.04% respectively. At the same time flexible DSSC with N-CNT/ITO/Polyethylene naphthalate substrate yielded an overall efficiency of 2.85%[144d]. However more efforts are required to increase the cell efficiency of flexible DSSC. Malara et al. have fabricated free standing, flexible counter electrode by transferring vertically aligned CNT forest onto oxygen plasma treated conductive nano-composite film. Firstly, an Al foil was taken onto which CNTs were grown via CVD. Nanocomposite film was fabricated via, dispersing CNTs onto polypropylene film which was then extruded to form pellets of CNT/Polypropylene. This was later prepared as a film and was etched with oxygen plasma to remove the polymer content. The Al/CNT film was later hot pressed onto the NC film which was used as a counter electrode. This system gave an efficiency of 7.26%[144f].

CNT/GRAPHENE COMPOSITE

Velten et al successfully fabricated multi walled carbon nanotube (MWCNT)/ graphene flakes (GF) composite as a possible replacement for Pt counter electrode. This composite showed an efficiency of 7.55% when compared to independently used MWCNT (6.62%) and GF (4.65%). CNT were synthesized via CVD and graphene through modified Hummer process. Firstly the CNT were transferred onto a FTO glass layer by layer. Grpahene solution was dropped on top of the CNTs sheet and was put in oven to evaporate excess solution. This process was repeated till the CNT were 5 layers and graphene solution of totally 0.35mL was drop casted. The CNT/graphene composite had additional surface area when compared to independent CNT, which acts as a good catalyst for the electrolyte[144e].

GRAPHENE

The 2-D graphene sheets, an allotrope of carbon containing covalently bonded sp^2 hybridized carbon atoms, exhibit unique electronic as well as catalytic activity.[145-147] Wang et al. developed a transparent, conductive graphene electrode for DSCs. These graphene thin films deposited on the hydrophilic substrates like quartz exhibited a high conductivity of 550 S/cm and a transparency of more than 70% in the wavelength of 1000-3000 nm.[148] There are various methods by which graphene based counter electrodes for DSSC could be made namely electrophoretic deposition,[149] chemical reduction of graphene oxide by microwave irradiation,[150] etc. However the catalytic activity of the graphene sheets is mainly dependent on their structure. Kaniyoor et al. thermally exfoliated graphene from graphite oxide. The graphene sheets thus obtained were highly wrinkled and had a surface area of about 470 m^2/g and the DSSC thus fabricated showed a conversion efficiency of 2.82%.[151] Though the 2-D graphene sheets possess very high surface area and high electrical conductivity, defect free graphene sheets are not suitable for better device performance. Thus always a good balance between the electrical conductivity and catalytic activity towards the reduction of the redox couple is required to be used as counter electrodes in DSSC. The active sites for the reduction of the redox couple are mostly the defects and the surface functional groups located at the crystal edges.[137,152-153] Kaven et al. used defect rich graphene nanoplatelets drop-casted on FTO as a counter electrode. Under one Sun illumination the DSSC thus fabricated with graphene nanoplatelets as counter electrode showed an efficiency of 4.4% and a fill-factor 0f 0.60.[154] Roy- Mayhew et al. had successfully demonstrated that the catalytic activity towards the I_3^- reduction can be tuned by increasing the amount of oxygen containing functional groups.[155] Doping the carbon materials with nitrogen introduces local strain in the hexagonal carbon network which in turn leads to structural deformations. Further the additional lone pair of electrons of the N atom brings about negative charge respect to the delocalized π system of the sp^2 hybridized carbon frame work. This can enhance both the electron transfer ability as well as the electrocatalytic activity.[156-157] Ju et al. have successfully fabricated DSSC with N-doped graphene nanoplatelets as counter electrodes and $Co(bpy)_3^{3+/2+}$ redox couple. They have reported the highest photovoltaic conversion efficiency of

9.05%. Figure 38 a shows the schematic of the synthesis of N-doped graphene nanoplatelets and their SEM image.[158]

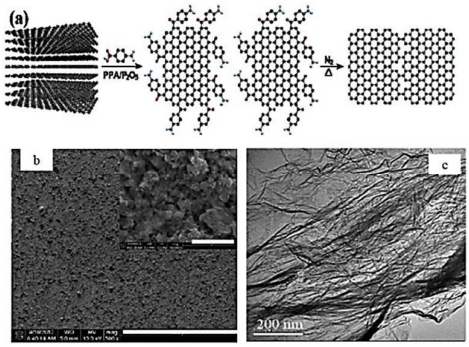

Fig. 38.a) schematic of synthesis of N doped graphene [158], b) SEM image of N- doped graphene [158] and c) TEM image of thermally exfoliated graphene. [151]

COMPOSITES WITH GRAPHENE

Graphene/polymer composite

The first composite based on grahene/polymers was first reported by Stankovich[159] following which several composites of graphene with conductive polymers have been reported for various applications. Composite film of graphene/PEDOT-PSS was synthesized by Hong et al. to be used as counter electrodes in DSSCs. The PEDOT-PSS acts as a conductive support in which the graphene sheets are dispersed uniformly due to the strong interactions between the 1-pyrenebutyrate (PB^-) functionalized graphene and the positively charged PEDOT chains. The thin graphene sheets with high specific surface area and chemical defects acts as a catalyst towards tri-iodide reduction whereas the PEDOT-PSS acts as a conductive matrix around the graphene. The energy conversion efficiency of the DSSC turned out to be 4.5%.[160] Graphene/Polyaniline nanocomposites as counter electrode was reported by Wang et al. In this composite the graphene sheets acts as the supporting medium in which the polyaniline nanoparticles were coated uniformly. The homogeneous and uniform dispersion of the PANI nanoparticle enhances both the conductivity and the catalytic activity. The energy conversion efficiency of the DSSC turned out to be 6.09%.[161] Benlin et al. synthesized PANI/graphene composite by a reflux technique. The lone pair of electrons of –NH- is shared with the carbon atoms forming covalent bond which accelerates the charge transfer along the PANI chains. The composite with 8 wt.% graphene showed the best performance with 7.78% as the conversion efficiency.[162] A cationic polymer PDDA decorated electrochemically reduced graphene oxide as counter electrode in DSSC was reported by Xu et al. The composite was synthesized by a layer-by-layer self-assembly technique. The composite showed enhanced electrocatalytic activity due to the electron withdrawing ability of PDDA. The DSSC thus fabricated with this composite as counter electrode and Z946 as electrolyte showed fill-factor and conversion efficiency of 0.74 and 9.14%, respectively.[163] Similarly polypyrrole nanoparticles of size 20-30 nm embedded reduced graphene oxide in which polypyrrole nanoparticles act as catalytic active centers showed photovoltaic performance comparable with that of the Pt-based counter electrodes.[164]

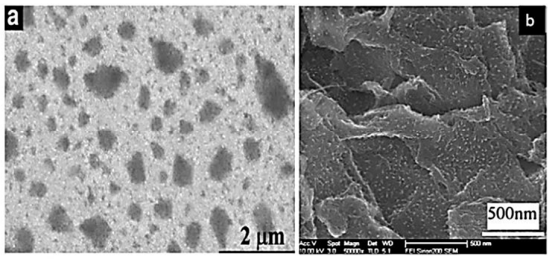

Fig. 39.SEM images of a) grepehene/PEDOT:PSS composite[160] and b) graphene/PANI composite[161]

Graphene/metal composites

In addition to the composites of graphene with polymers, composites of graphene with metals had also been widely investigated. Ni is a transition metal with good catalytic activity and it also exhibits high stability in the I_2+LI electrolyte.[165-166] Bajpai et al. synthesized Ni nanoparticle/graphene composite in which the Ni nanoparticles were deposited on the surface of the graphene platelets. The Ni nanoparticles acted as active catalyst which is reflected in the stronger I_3^- reduction peak in the cyclic voltammetry scans and the efficiency of the cell turns out to be 2.19%.[167] The DSSC fabricated with graphene-Pt nanoparticle-based counter electrode showed an efficiency of 6.77%. There are two pairs of peaks observed in the cyclic voltammetry corresponding to oxidation and reduction. The reduction processes are

$$I_3^- + 2e^- \rightarrow 3I^-$$
$$3I_2 + 2e^- \rightarrow 2I_3^-$$

Tjoa et al. have also shown that an optimized balance between the conductivity and the catalytic activity is required for the best device performance.[168] Gong et al. employed electrostatic layer-by-layer self-assembly technique to synthesize graphene/Pt monolayer to be used as counter electrode in DSSC. The device achieved 7.6% conversion efficiency. Since it employs a simple technology making use of a little amount of Pt, the overall cost of the device is reduced thus facilitating production in large scale.[169]

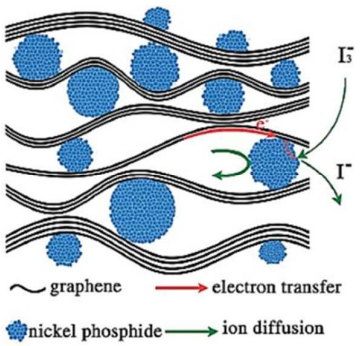

Fig. 40. Electron transport mechanism in graphene/metal composite.[171]

Gou et al. reported Nickel phosphide-graphene composite to be used as counter electrode. In this composite, the graphene ensures better electrode-electrolyte contact and also provides a fast diffusion pathway for the electrons. The $Ni_{12}P_5$ nanocrystallites not only act as active sites for electrocatalytic processes but also as spacers among the graphene layers thus activating the diffusion of the electrolyte species. The photovoltaic parameters V_{oc}, J_{sc}, FF and η for DSSC fabricated are 0.727V, 12.86 mA/cm^2, 0.61 and 5.70%, respectively.[170]

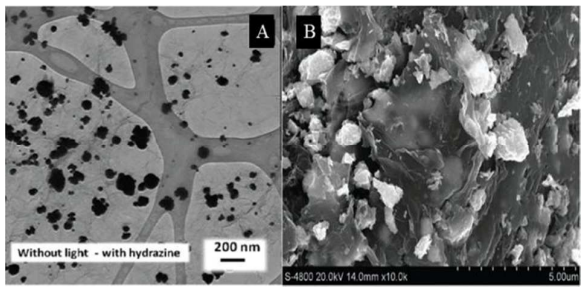

Fig. 41.SEM image of A) Graphene/ Pt. composite[168] and B) graphene/$Ni_{12}P_5$ [171]

NINE KINS OF CARBON

Wu et al. compared the performance of DSSC with counter electrodes based on nine different kind of carbon materials namely activated carbon (Ca), carbon black (Cb), carbon nanotube (Cn), conductive carbon (Cc), carbon dye (Cd), carbon fiber (Cf), mesoporous carbon (Cm), discarded toner of a printer (Cp) and fullerene (C_{60}). From the cyclic voltammetry study it was found that the counter electrodes based on mesoporous carbon and carbon dye exhibits a large current density thus indicating a high electrochemical activity and both the materials showed energy conversion efficiencies comparable with that of platinum. Thus carbon dye with small size and large surface area obtained by incomplete combustion of the coal tar proves to be a low cost alternative counter electrode material for DSSC.

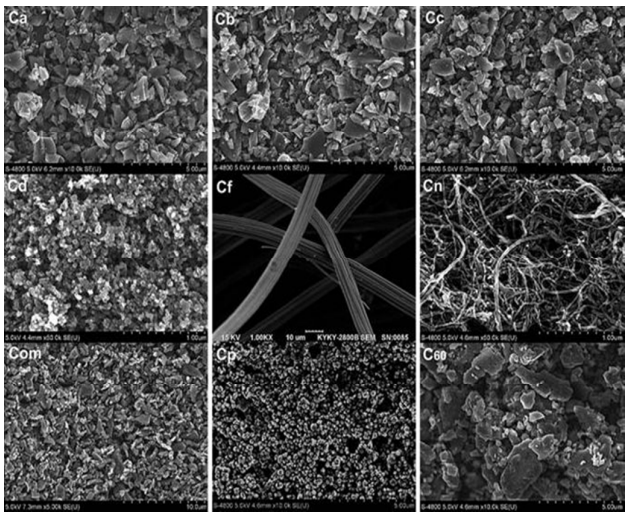

Fig. 42.SEM images of 9 different kinds of carbon[170].

The lower diffusion co-efficient and diffusion limited current density were responsible for the inferior photovoltaic performance of DSSC with the fullerene-based counter electrodes. Toner is in general a mixture of carbon powder and iron oxide and it is used in laser printers. The DSSC with this material as counter electrode showed an efficiency of 4.3% and thus it is another cheaper alternative making use of discarded toner and thus comes under the category of waste reutilization.[171]

FORM OF CARBON	Voc (V)	Jsc (mA/cm^2)	FILL FACTOR	EFFICIENCY
Carbon black[121]	0.78	16.8	0.68	9.1%
Mesoporous carbon[125]	0.6	15.5	0.65	6.18%
Nanocarbon[123]	0.74		0.62	6.73%
Activated carbon nanofiber[130]	0.73	15.4	0.64	7.21%
MWCNT[136]	0.78	15.64	0.62	7.59%
Core- shell porous carbon structure[128]	0.74	15.81	0.67	7.56%
Graphene[151]	0.68	7.7	0.54	2.82%
Graphene nanoplatelets[155]	0.67	11	0.60	4.38%
N doped graphene nanoplatelets[158]	0.88	13.83	0.74	9.02%
Inverse opal carbon[127]	0.77	11.04	0.64	5.49%
Sub micrometer graphite[132]	0.79	12.7	0.62	6.2%
Graphene/Pt nanoparticles[169]	0.71	15.20	0.71	7.66%
Graphene/$Ni_{12}P_5$[170]	0.73	12.86	0.61	5.70%

Table 4. Summary of Photovoltaic parameters of DSSC with different carbon counter electrode.

Non planar wire shaped DSSC

One of the major disadvantages of the planar DSSC is the higher leakage rate of the electrolyte due to the large contact area between the electrolyte and the sealing material. Due to the thermal dilation, deformation and strain, two assembled planar electrodes tend to break at the interface[172-173]. In addition to high surface area, good electrical conductivity and electrocatalytic properties, these carboneous materials also exhibit high stability and good flexibility. Thus these carboneous materials play an important role in fabricating flexible solar cells in order to meet the requirement of portable electricity and roll to role industrial fabrication[174-175]. Recently non planar DSSC with 3D structure have attracted great deal of attention due to facile integration of these modules using textile technology[176]. Flexible fiber shaped DSSC fabricated with pure commercial carbon fiber as counter electrode showed a cell efficiency of 2.7% which was further improved to 5.8% by platinizing it[177]. Zhang et al. developed Pt nanoparticle adsorbed carbon nanotube yarns to be used as

counter electrode in flexible fiber shaped DSSC. Pt nanparticles had been adsorbed onto free standing CNT fiberweb and the hybrid film was spun into yarn. The uniform distribution of the Pt nanoparticles onto the porous carbon nanotube yarn increases the effective catalytic sites and thus the overall cell performance. The DSSC fabricated with this composite material with 0.7wt% Pt loading as counter electrode showed a cell efficiency of 4.85%. The cell performance was also dependent on the diameter of the yarn. Thicker yarns with more number of nanotubes have larger number of catalytic active sites which aids in enhancing the cell performance. However beyond a certain thickness the efficiency is pulled down due to the limited diffusion of the electrolyte into the inner portion of the CNT network and the blocking of the incident light. The best performance was shown by yarns with 90µm diameter having R_{ct} value of 214.8Ω. From the mechanical stability aspect, the cell efficiency was stable over repeated bending to 180° for 500 cycles[178].

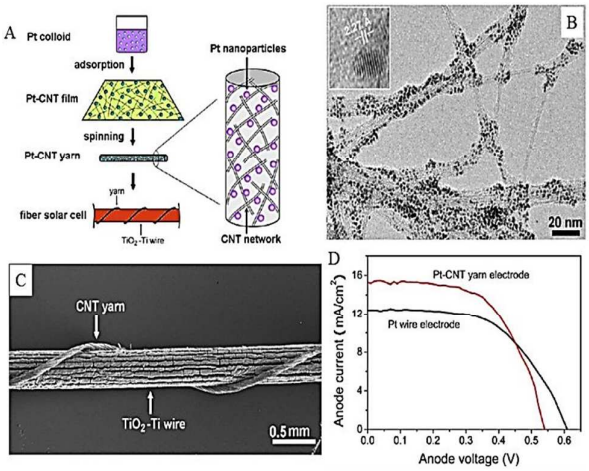

Fig. 43.A) Schematic showing the synthesis procedure, B) TEM image of CNT- Pt Nanoparticle, C) SEM image a.d D) J-V characteristics[178].

Hou et al. synthesized carbon fiber/PEDOT PSS composite material with highly ordered carbon fiber conductive core and PEDOT PSS films as the catalytic shells to be used as counter electrode in wire shaped DSSC. Due to the good flexibility of the composite it can be easily wrapped along a Ti wire based photoanode. From the CV measurements it was found that CF/PEDOT composite showed higher electrochemical stability than the carbon fiber/Pt electrode and the DSSC fabricated showed a highest conversion efficiency of 5.5%[179]. The first all carbon based fiber shaped dye sensitized solar cell was demonstrated by Cai et al. The photoanode has a core shell structure with a carbon fiber core and TiO_2 film as a shell. The sensitized TiO_2 aids in light harvesting whereas the conductive carbon core collects the charges. The counter electrode was made of carbon fiber covered with carbon ink on the surface. The ink carbon particles with relatively large specific surface area of 32.78 m^2/g showed excellent catalytic activity towards the tri- iodide reduction. The fiber shaped DSSC with 2.5cm length showed an efficiency of 1.09%. As we know the V_{oc} is the potential difference between the fermi level of TiO_2 and the redox potential of the electrolyte. However in the presence of the carbon fiber, since the workfunction of carbon fiber is much deeper than that of the conduction band of the TiO_2, the contact between carbon fiber and TiO_2 causes a negative shift in the Fermi level of TiO_2 and as a result, reduction in the V_{oc}. Thus the device performance can be enhanced by tuning the interface barrier of carbonfiber/TiO_2.[180]

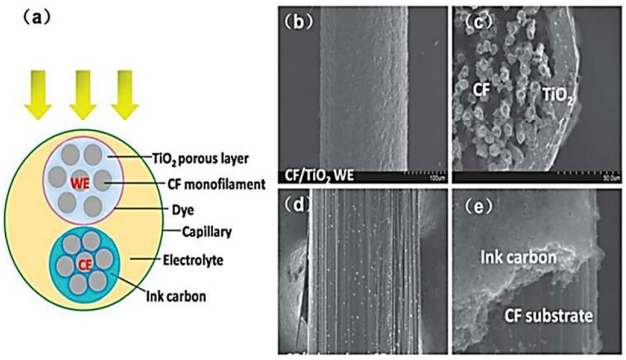

Fig.44. (a) Schematic showing all carbon electrode DSSC. SEM image top view (b) and cross sectional view (c) of carbon fiber/TiO_2 photoanode, top view (d) of carbon fiber ink carbon and (e) carbon fiber substrate and ink carbon SEM image[180].

Interwined aligned carbon nanotube fiber based dye sensitized solar cell was reported by Chen et al. the device was fabricated by interwining dye absorbed CNT/TiO_2 composite fiber with bare CNT fiber which acts as a counter electrode. They have achieved a power conversion efficiency of 2.94%. The device performance was highly dependent on the twining structure and if the electrodes are twined tightly, it may cause short circuiting and the efficiency is drastically reduced if they are twined loosely. Since the cell efficiency was independent of the cell length and the incident light it may be scaled up easily for various potential applications[181].

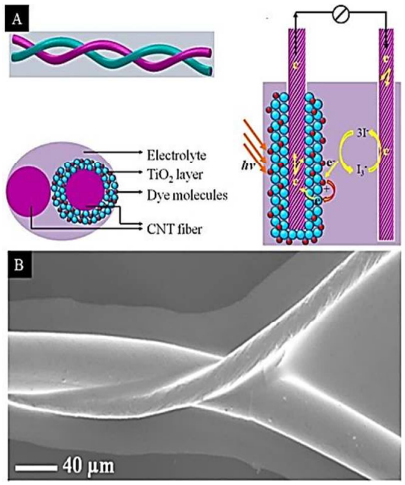

Fig. 45.A) Schematic showing the interwined carbon nanotube fiber based fiber shaped DSSC and B) SEM image of the twined structure[181].

Pan et al. have fabricated and compared the performance of wire shaped DSSC with four different types of carbon nanostructures namely carbon nanotubes, core- sheath CNT/ Reduced graphene oxide nanoribbon (RGONR), CNT/RGO and RGO fibers as counter electrode. Among the four different nanostructures the core- sheath CNT/RGONR showed the highest energy conversion of 5.64%. The electrocatalytic activity is also dependent on the type of the electrolyte used. For the organic T^-/T_2 electrolyte, the CNT fiber counter electrode showed the best performance with 4.78% energy conversion efficiency. From the cyclic voltammetry studies it had been found that the electrocatalytic activity towards the tri- iodide reduction increased from RGO fiber, CNT/RGO composite, CNT fiber to core- sheath/RGONR. The high electrical conductivity of aligned CNT core (380 S/cm) and the active edge site of the RGONR for catalysis are responsible for the the best performance of the device. However for the T^-/T_2 reduction, the presence of RGO in the core- sheath/ RGONR hinders the infilteration of organic T^-/T_2 redox into the fibers resulting in lower catalytic activity[182].

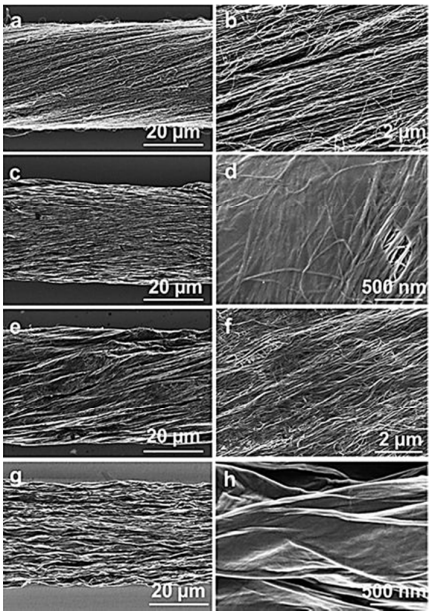

Fig. 46. SEM images low and high magnification of CNT fiber (a,b), core-sheath CNT/RGO composite (c,d), CNT/RGO composite (e,f) and RGO fiber (g,h) respectively[182].

Conclusions

Due to the two dimensional π conjugated structure and excellent electron conductivity, graphene proves to be a competitive acceptor[183] and superior charge transport material.[184] Thus both the outstanding acceptor and the transport properties of the graphene are responsible for efficient charge separation and transportation of the electrons. Since the work function of the carbon nanostructures such as graphene and the carbon nanotubes is more negative than that of the TiO_2, the favourable band alignment aids in opening additional electron transport channel for the flow of electrons. Graphene also acts as a superior light scattering layer scattering light in the visible region of the spectrum.[106] However as the concentration of the carbon nanostructures increases the photovoltaic performance decreases. Thus always an optimal concentration of the carbon nanostructures is required. This is because as the concentration of carbon nanostructures increases, agglomeration of the particles on the surface increases which reduces the specific surface area of the film. As a result the quantity of dye that is absorbed also decreases.[185] Further a red-shift in the absorption onset is also observed with the increase in the concentration of the carbon nanostructures due to the formation of Ti-O-C bond which leads to the narrowing of the band-gap of TiO_2 leading to visible light absorption.[186] This in turn leads to the light harvesting competition between the dye and the composite.[187] There are two ways by which the carbon nanostructures/TiO_2 composite could be made. In the first case carbon is added to TiO_2 till a percolation network is formed and in the second case, TiO_2 is deposited on the surface of the carbon nanostructure. However since the metal oxide i.e. TiO_2 acts as the photoactive material onto which the dye anchors, there must be uniform immobilization and adhesion of the metal oxide on the surface of the carbon nanostructures for better dye loading and light harvesting. Hence uniform immobilization of TiO_2 on the carbon nanostructure surface proves to be a promising approach for further improvement. Although the efficiency of the DSSC had achieved the level needed for commercialization, the counter electrode made of Platinum which is an expensive noble metal must be replaced to reduce the overall device cost. An ideal counter electrode must exhibit long term stability and high electrocatalytic activity. The carbon nanostructures with high surface area and unique electrical properties prove to be a suitable alternative for the Pt-based counter electrodes. Several carbon nano structures have been used either independently or as composite with other metal to be used as a replacement for Pt. In-addition, due to the flexible nature of these carboneous materials, non-planar flexible solar cells for portable electronic devices has also been fabricated. However, the efficiency of these wire shaped devices are not comparable with that of the conventional planar DSSC. Due, to the mismatch in the band-gap between these carbon materials and TiO_2, the V_{OC} is highly compromised, which is one of the major reasons for the poor performance of the flexible devices. This in turn restricts the commercialization of these products. Further investigation in the lines of tuning the band alignment as well as, retaining the structural integrity and flexibility can be a future scope for the commercialization of DSSC.

Acknowledgements

The authors thank Ministry of New and Renewable Energy (MNRE), Govt. of India and Solar Energy Research Initiative (SERI) of the Department of Science and Technology, Govt. of India for financial support.

References

1 W. West, *Photogr. Sci*. Eng., 1974, **18**, 35-48.
2 H. Gerisher, H. Tributsh, Ber. Bunsen, *Phys. Chem*., 1968, **72**, 437-445.
3 H. Tributsh, H. Gerisher, Ber. Bunsen, *Phys. Chem*., 1969, **73**, 251-260.
4 M.T. Spitler and M. Calvin, *J. Chem. Phys*., 1977, **66**, 4294-4305.
5 B.O'Regan and M.Gratzel, *Nature.*, 1991,**353**,737.
6 P. Liska, N. Vlachopoulos, M. K. Nazeeruddin, P. Comte and M. Graetzel, J. Am. Chem. Soc., 1988, **110**, 3686- 3687.
7 M. K. Nazeerudin, A.Kay, I rodicio, R Humpry- Baker, E. Muller, P. Liska, N. Vlachopoulos and M. Gratzel, *J. Am. Chem. Soc.*, 1993, **115**, 6382-6390.
8 M. K. Nazeeruddin, P.Pechy and M. Gratzel, *Chem. Commun.*, 1997, 1705-1706.
9 Brian O'Regan, J. Moser, M.Anderson and M. Graztel, *J.Phys. Chem.*, 1990, **94**, 8720-8726.
10 S. Sodergren, A. Hagfeldt, J. Olsson and S. Lindquist, *J.Phys.chem*., 1994, **98**, 5552-5556.
11 A. Hagfeldt, G. Boschloo, L. Sun, L. Kloo and H. Petterson, *Chem.Rev.,* 2010, **110**, 6595-6663.
12 K. G. Reddy, T. G. Deepak, G. S. Anjusree, S. Thomas, S. Vadukumpully, K. R. V. Subramaniam, S. V. Nair and A. S. Nair, *Phys. Chem. Chem. Phys.*, 2014, **16**, 6838-6858.
13 S. Yang, D. Yang, J. Kim, J. Hong, H. Kim, I. Kim and H. Lee, *Adv. Mater*., 2008, **20**, 1059-1064.
14 F. Huang, D. Chen, X. Zhang, R. A. Caruso and Yi-Bing Cheng, *Adv.Func.Mater*., 2010, **20**, 1301-1305.
15 Y. Diamant, S. Chappel, S.G. Chen, O. Melamed and A. Zaban, *Co ord. Chem. Rev*., 2004, **248**, 1271-1276.
16 M. Adachi, Y. Murata, J. Takao, J. Jiu, M. Sakamoto, and F. Wang, *J.Am.Chem.Soc.,* 2004, **126**, 14943-14949.
17 K. Fujihara, A. Kumar, R. Jose, S. Ramakrishna and S. Uchida, *Nanotechnology*, **18**, 2007, 365709.
18 D. Kuang, J. Brillet, P. Chen, M. Takata, S. Uchida, H. Miura, K. Sumioka, S.M. Zakeeruddin and M. Graztel, *ACS Nano*, 2008, **6**, 1113-1116.
19 A.S. Nair, R. Jose, Y. Shengyuan, and S. Ramakrishna, *J. Colloid Interface. Sci.,* 2011, **353**, 39-45.
20 P. Joshi, L. Zhang, D. Davoux, Z. Zhu, D. Galopeau, H. Fong and Q. Qiao, *Energy Environ.Sci*., 2010, **3**, 1507-1510.
21 B. Tan and Y. Wu, J.Phys.Chem.B., 2006, **111**, 15932-15938.
22 A) A. S. Nair, Z. Peining, V. J. Babu, Y. Shengyuan and S. Ramakrishna, *Phys. Chem. Chem. Phys*., 2011, **13**, 21248-21261. B) A. Jena, S.P. Mohanty, P. Kumar, J. Naduvath, V. Gondane, P. Lekha, J. Das, H. K. Narula, S. Mallick and P. Bhargava., *Trans. Ind. Ceram. Soc.,* 2012, **71,** 1-16.
23 S. Chappel, L. Grinis, A. Offir, and A. Zaban, *J.Phys.Chem.B*., 2005, **109**, 1643-1647.
24 a) D. E. Soule, *Phys. Rev*., 1958, **112**, 698. b) G. Fugallo, A. Cepellotti, L. Paulatto, M. Lazzeri, N. Marzari and F. Mauri, *NanoLett.,* 2014, **14**, 6109-6114,
25 a) K.I. Bolotin, K.J. Sikes, Z. Jiang, M. Klima, G. Fudenberg, J. Hone and P. Kim, *Solid state communication*., 2008, **146**, 351-355. b) A. Balandin, S. Ghosh, W. Bao, I. Calizo, D. Teweldebrhan, F. Miao and C. Lau, *NanoLett*., 2008, **8**, 902-907.
26 a) G. Pennington and N. Goldsman, *Phys Rev. B*., 2003, **68**, 045426. b) S. Berber, Y. Kyun Kwon and D. Tamonek, *Phy. Rev. Lett*, 2000, **84**, 4613.
27 Th. B. Singh, N. Marjanovic, G. J. Matt, S. Gunes, N.S. Sariciftci, A. Montaigne Ramil, A. Andreev, H. Sitter, R. Schwodiauer and S. Bauer, *Organic electronics* 2005, **6**, 105-110.
28 J. Tsai and J. Tu, *Materials and Design*, 2010, **31**, 194-199.
29 Y. Wu, X. Zhang, A. Y. T. Leung and W. Zhong, *Thin walled structures*., 2006, **44**, 667-676.
30 T. Natsuki, K. Tantrakarn and M. Endo, *Carbon*., 2004, **42**, 39-45.
31 M. M. Shokreih and R. Rafiee, *Materials and Design*., 2010, **31**, 790-795.
32 K. Saito, K. Miyazawa and T. Kizuka, *J. Appl. Phys*., 2009, **48**, 010217.
33 A. R. Oganov, R. J. Hemley, R. M. Hazen and A. P. Jones, *Reviews in Mineralogy & Geochemistry*, 2013, **75**, 47-77.
34 X. Hu, K. Huang, D. Fang and S. Liu, *Material Science and Engineering B*., 2011, **176**, 431.
35 Y. S. Park and H. K. Kim, *Current Applied Physics*, 2011, **11**, 789.
36 E. Ramasamy and J. Lee, *Carbon*, 2010, **48**, 3715.
37 J. Zhang, X. Li, W. Guo, T. Hreid, J. Hou, H. Su and Z. Yuan, *Electrochimica Acta*, 2011, **56**, 3147.
38 C.T. Hseih, B.H. Yang and J.Y. Lin, *Carbon*, 2011, **49**, 3092.
39 M.Y. Yen, M.C. Hsiao, S.H. Liao, P.I. Liu, H.M. Tsai, C.C.M.Ma, N.W. Pu and M.D. Ger, *Carbon*, 2011, **49**, 3507.
40 W. Hong, Y. Xu, G. Lu, C. Li and G.Shi, *Electrochemistry communications*, 2008, **10**, 1555.
41 L. Wan, S. Wang, X. Wang, B. Dong, Z. Xu, X. Zhang, B. Yang, S. Peng, J. Wang and C. Xu, *Solid state Sciences.*, 2011, **13**, 468.
42 G. Zhu, T. Xu, T. Lv, L. Pan, Q. Zhao and Z. Sun, *Jounrnal of electroanalytical chemistry*., 2011, **650**, 248.
43 S. Giljie, S.Han, M. Wang, K.L.Wang and R.B. Kaner, *NanoLett*., 2011, 7, 3394
44 K. S. Novoselov, A. K. Gelm, S.V. Morozov, I. V. Grigorieva and A. A.Firsov, *Science*, 2004, **306**, 666-669.
45 A. K. Geim and K. S. Novoselov, *Nat. Mater.,* 2007, **6**, 183-191.
46 K.S. Novoselov, A. K. Gelm, S. V. Morozov, D. Jiang, M. I. Katsnelson, I. V.Grigorieva, S. V. Dubonos, and A. A. Firsov, *Nature*, 2005, **438**, 197- 200.
47 Y. Zhang, Y. W. Tan, H. L. Stormer and P. Kim, *Nature* 2005, **438**, 201- 204.
48 M. J. Allen, V. C. Tung and R. B. Kaner, *Chem. Rev*., 2010, **110**, 132-145.
49 X. L. Li, X. Wang, L. Zhang, S. Lee, H. J. Dai, *Science*, 2008, **319**, 1229- 1232.
50 X. L. Li, G. Y. Zhang, X. D. Bai, X. M. Sun, X. R.Wang, E. G. Wang and H. J. Dai, *Nat. Nanotechnology*., 2008, **3**, 538- 542.
51 Y.B. Tang, C. S. Lee, Z. H. Chen, G. D. Yuan, Z. H. Kang, L. B. Luo, H. S. Song, Y. Liu, Z. B. He, W. J. Zhang, I. Bello and S. T. Lee, *NanoLett*., 2009, **9**, 1374-1377.
52 S. Gilje, H. Song, M. Wang, K. L. Wang and R. B. Kaner, *Nano Lett*., 2007, **7**, 3394-3398.
53 G. Eda, G. Fanchini and M. Chhowalla, *Nat. Nanotechnol*., 2008, **3**, 270-274.
54 G. Williams, B. Seger and P. V. Kamat, ACS Nano, 2008, **2**, 1487-1491.
55 P. J. F Harris,Carbon Nanotubes and Related Structure: New Material for the twenty first century, Cambridge University Press, 1999, Cambridge.
56 V. N. Popov, Carbon Nanotubes: properties and application, Material science and Engineering R, 2004, **43**, 61-102.
57 M.Endo, S. Iijima and M. S. Dresselhaus (Eds) 1996 Carbon Nanotubes. Pergamon , New York.
58 S. J. Tans, A. R. M. Verscheuren and C. Dekker, *Nature*, 1998, 398, 49-52.
59 H. Dai and J. H. Haffner, *Nature*, 1996, 384, 147-151.
60 T. Reuckes, K. Kim, E. Joselevich, G. Y. Tsang and C. L. Cheung, *Science* 2000, **289**, 94-97.
61 B J Hinds, N Chopra and T Rantell Science, 2004, **393**, 346-9.
62 Y. Saito, K. Hamaguchi, Jpn. J. Appl.Phys., 1997, **36,** L1340.

63 L. Dai, P. Soundarrajan and T. Kim, *Pure.Appl.Chem*., 2002, **74**, 1753-72
64 G. Eda and M. Chhowalla, *Nano Lett*., 2009, **9**, 814-818.
65 S. Watcharaotone, D. A. Dikin, S. Stankovich, R. Piner, I. Jung, G. H. B. Dommet, G. Evmenenko, S. E. Wu, S. F. Chen, C. P. Liu, S. T. Nguyen, R. S. Ruoff, *NanoLett.* 2009, **7**, 1882-1892.
66 K. H. Jung, S. R. Jang, R. Vittal, D. Kim and K.J. Kim, *Bull. Korean Chem Soc*., 2003, **24**, 1501-1504.
67 S. L. Kim, S. R. Jang, R.Vittal, J. Lee and K. J. Kim, *Journal of Applied electrochemistry* 2006, **36**, 1433-1439.
68 T. Sawatsuk, A. Chindaduong, C. Sae-kung, S. Pratontep and G. Tumcharern, *Diamond and related materials*, 2009, **18**, 524-527.
69 T. Y. Lee, P.S.Alegaonkar and Ji-Beon Yoo, *Thin solid films*, 2007, 515, 5131-5135.
70 S. R. Jang, R.Vittal and K. J. Kim, *Langmuir*, 2004, 20, 9807-9810.
71 K. M. Lee, C.W. Hu, H.W. Chen, K. C. Ho, *Solar energy materials and solar cells*, 2008, **92**, 1628-1633.
72 S. Zhang, H. Niu, Y. Lan, C. Cheng, J. Xu and X. Wang, *J.Phys.Chem.C* 2011, **115**, 22025-22034.
73 J. Yu, J. Fan and B. Cheng, *J. Power sources*, 2011, **196**, 7891-7898.
74 S. Muduli, W. Lee, V. Dhas, S. Mujawar, M. Dubey, K. Vijayamohan, S. Han and S. C. Ogale, *ACS Appl. Mater. Inter*., 2009, **1**, 2030-2035.
75 X. Dang, H. Yi, M. H. Ham, J. Qi, D. S. Yun, R. Ladewski, M. S. Strano, P. T. Hammord, and A. M. Belcher, *Nature Nanotechnology*, 2011, **6**, 377-384.
76 S. Sadhu, P. Poddar, *J. Phys. Chem. C*, 2014, **118**, 19363-19373.
77 H. Chang, T.J. Hsieh, T. L. Chen, H. S. D. Huang, C. S. Jwo and S. H. Chein, Materials transcations, 2009, **50**, 2879-2884.
78 P. Brown, K. Takechi and P. V. Kamat, *J. Phys. Chem. C*, 2008, **112**, 4776- 4782.
79 Z. Peining, A. S. Nair, Y. Shengyuan, P. Shengjie, N. Elumalai, S. Ramakrishna, *Journal of Photochemistry and photobiology A: Chemistry,* 2012, **231**, 9-18.
80 S. Zhang, C. Ji, Z. Bian, R. Liu, X. Xia, D. Yun, L. Zhang, C. Huong and A. Cao, *Nano Lett*., 2011, **11**, 3383-3387.
81 G. Williams,B. Seger, P. V. Kamat, ACS Nano 2008, **2**, 1487-1491
82 N. Yang, J. Zhai, Y. Chen, and L. Jiang, ACS Nano 2010, **4**, 887-894.
83 L. Chen, Y. Zhou, W. Tu, Z. Li, C. Bao, H. Dai, T. Yu, J. Liu and Z. Zou, *Nanoscale*, 2013, **5**, 3481-3485.
84 Y. Tang, C. Lee, J. Xu, Z. T. Liu, Z. H. Chen, Z. He, Yu-Lin Cao, G. Yuan, H. Song, L. Chen, L. Luo, H. M. Cheng, W. J. Zhang, I. Bello, and S.T. Lee, *ACS Nano*, 2010, **6**, 3482-3488.
85 L. Chen, Y. Zhou, W. Tu, Z. Li, C. Bao, H. Dai, T. Yu, J. Liu and Z. Zou, *Nanoscale*, 2013, **5**, 3481-3485.
86 Y. Liu. Y. Cheng, W. Shu, Z. Pong, K. Chen, J. Zhou, W. Chen and G. S. Zakharova, *Nanoscale*, 2014, **6**, 6755-6762.
87 T. H. Tsai, S. C. Chiou and S.M. Chen, *Int. J. Electrochem. Sci*., 2011, **6**, 3333-3343.
88 W. Hailiang, T. R. Joshua, D. Georgi and D. Hongie, J. Am. Chem. Soc., 2010, **132**, 3270.
89 G. S. Anjusree, A. S. Nair, S. V. Nair and S. Vadukumpully, *RSC Adv.,* 2013, **3**, 12933-12938.
90 Z. He, G. Gai, J. Liu, C. Guo, J. S. C Loo, C. M. Li and T. Thatt, Y. Tan, Nanoscale, 2011, **3**, 4613-4616.
91 W. Shu, Y. Liu, Z. Peng, K. Chen, C. Zhang, W. Chun, *Journal of alloys and compounds*, 2013, **563**, 229-233.
92 J. Chang, J. Yang, P. Ma, D. Wu, L. Tian, Z. Gao, K. Jiang and L. Yang, *Journal of colloidal and interface science*, 2013, **394**, 231-236.
93 S. Sun, L. Gao and Y. Qiao, *Appl.Phys.Lett*., 2010,**96**, 083113.
94 B. Roy, S. P. Ahrenkeil and P. A. Fuierer, *J. Am. Ceram. Soc.*, 2008, **91**, 2455.
95 A. A. Madhavan, R. Ranjusha, K.C. Daya, P. Praveen, K.P. Sanosh, K.R.V. Subramanian, S. V.Nair and A. Balakrishnan, *Sci. Adv. Mater*., 2014, **6**, 1-7.
96 X. Feng, K. Shankar, O. K. Varghese, M. Paulose, T. J.Latempa and C. A.Grimes, *NanoLett*, 2008, **8**, 3781-3786.
97 B. Tan and Y. Wu, *J. Phys. Chem. B*, 2006, **110**, 15932-15938.
98 Z. Peining, A. S. Nair, P. Shengjie, Y. Shengyuan and S. Ramakrishna, *ACS Appl. Mater. Interfaces* 2012, **4**, 581-585.
99 A. A. Madhavan, S. Kalluri, D. K. Chacleo, T. A. Arun, S. Nagarajan, K.R.V. Subramanian, A.S. Nair, S.V. Nair and A. Balakrishnan, *RSC Adv*.,2012, **2**, 13032-13037.
100 Y. Wang, Z. Li, Y. Tian, W. Zhao, X. Liu and J. Yang, *J. Mater Sci*, 2014, **49**, 7991-7999.
101 X. Luan, D. Guan and Y. Wang, *J. Phys Chem. C*, 2012, **116**, 14257.
102 D. Kim, A. Ghicov, S. P.Albu and P. Schmuki, *J. Am. Chem. Soc*. 2008, **130**, 16454-16455.
103 X. Luan, L. Chen, J. Zhang, G. Qu, J. C. Flake and Y. Wang, *Electrochimica Acta*, 2013, **111**, 216-222.
104 J.G.Yu, J.J. Fan and K.L.Lv, Nanoscale, 2010, **2**, 2144.
105 J. Fan, S. Liu and J. Yu, *J. Mater. Chem*., 2012, **22**, 17027-17036.
106 C. B. Song, Y.H. Qiang, Y.L. Zhao, X.Q. Gu, L. Zhu, J. Song and X. Liu, *Int. J. Elctrochem. Sci.*, 2014, **9**, 8090-8096.
107 B. Tang and G. Hu, *Journal of Power sources*, 2012, **220**, 95-102.
108 M.Y. Yen, M. C. Hsiao, S. H. Liao, P. I. Liu, H.M. Tsai, C. C. M. Ma, N. W. Pu, M. D. Ger, *Carbon*, 2011, **49**, 3597-3606.
109 H. Kim, G. Moon, D. M. Satoca, Y. Park and W. Choi, *J. Phys. Chem. C.*, 2012, **116**, 1535-1543.
110 X. Fang, M. Li, K. Guo, J. Li, M. Pan, L. Bai, M. Luoshean and X. Zhao, *Electrochimica Acta.,* 2014, **137**, 634-638.
111 E. Lee, J. Ryu and J. Jang, *Chem. Commun*., 2013, **49**, 9995-9997.
112 J. Liu, Y. T. Kuo, K. J. Klabunde, C. Rochford, J. Wu and Jun Li, *ACS Appl. Mater. Interfaces*, 2009, **1**, 1645-1649.
113 S. Ito, T. N. Murakami, P. Comte, P. Liska, C. Gratzel, M.K. Nazeerudin, M. Gratzel, Thin Solid Films 2008, **516**, 4613.
114 T. Chen, W. Hu, J. Song, G. H. Guai and C. M. Li, *Adv. Funct. Mater*. 2012, **22**, 5245-5250.
115 C. H. Hsu, J. R. Wu, L. C. Chen, P. S. Chan, C. C. Chen, Advances in Materials science and Engineering, **2014**, 2014.
116 S. R. Kim, Md. K. Parvez, M. Chhowalla, *Chemical Physics Letters*, 2009, **438**, 124-127.
117 E. Olsen, G. Hagen and S.E. Lindquist, *Sol. Energy. Mater. Solar cells*, 2000, **63**, 267-273.
118 A. Kay and M. Graztel, *Solar energy materials and the solar cells* 1996, **44**, 99-117.
119 H. S. Wroblowa and A. Saunders, *J. Electroanal. Chem. Interfacial Electrochem*., 1973, **42**, 329.
120 K. Kinoshita, Carbon, Electrochemical and Physiochemical Properties, Wiley- Interscience Publications, Newyork, 1987, 226- 379.
121 T. N. Murakami, S. Ito, Q. Wang, M. K. Nazeeruddin, T. Bessho, I. Cesar, P. Liska, R.H. Baker, P. Comte, P. Pechy and M. Graztel, *J. Electrochem. Soc.,* 2006, **153**, A2255-A2261.
122 K. Imoto, K. Takahashi, T. Yamaguchi, T. Komura, J. Nakamura and K. Murata, *Solar energy materials and solar cells*, 2003, **79**, 459-469.
123 E. Ramasamy, W. J. Lee, D. Y. Lee and J. S. Song, *Applied Physics Letters*, 2007, **90**, 173103.
124 J. Chen, K. Li, Y. Luo, X. Guo, D. Li, M. Deng, S. Huang, Q. Meng, *Carbon*, 2009, **47**, 2704-2708.
125 G. Wang, W. Xing and S. Zhuo, *Journal of Power sources,* 2009, **194**, 568-573.

126P. Joshi, L. Zhang, Q. Chen, D. Galipeau, H. Fong and Q. Qiao, *ACS Applied materials and interfaces*, 2010, **2**, 3572-3577.
127D. Y. Kang, Y. S. Lee, C. Y. Cho and J. H. Moon, *Langmuir*, 2012, **28**, 7033-7038.
128B. Fang, S. Q. Fan, J. H. Kim, N. K. Chaudri, J. Ko, and J. S. Yu, *Langmuir,* 2010, **26**, 11238-11243.
129G. Wang, W. Xing and S. Zhuo, *Materials Science Forum*, 2011, **685**, 1-5.
130a)S.H. Park, B. K. Kim, W. J. Lee, *J.Power Sources,* 2013, **239**, 122-127. b) A. Aboagye, H. Elbihy, A. D. Keljar, Q. Qiao, J. Zai, X. Qian and L. Zhang, Nano Energy 2015, **11**, 550-556. C) S. Sigdel, A. Dubey, H. Elbohy, A. Aboagye, D. Galipeau, L. Zhang, H. Fong and Q. Qiao, J. Mater. Chem. A, 2014, **2**, 11448.
131C. E. Banks, T. J. Davies, G. G. Wildgoose and R. G. Compton, *Chem. Commun*., 2005, **7**, 829-841.
132G. Veerapan, K. Bojan and S.W. Rhee, *ACS Appl. Mater. Interfaces,* 2011, **3**, 857-862.
133B.C. Yadav and Ritesh kumar, *International Journal of Nanotechnology and applications*, 2008, **2**, 15-24.
134T. Hino, Y. Ogawa and N. Kuramoto, *Carbon,* 2006, **44**, 880-887.
135K. Suzuki, M. Yamaguchi, M. Kumagai and S. Yamagida, *Chemistry Letters*, 2003, **32**, 28-29.
136E. Ramasamy, W. J. Lee, D. Y. Lee and J. S. Song, *Electrochemistry communications*, 2008, **10**, 1087-1089.
137J. E. Trancik, S. C. Barton and J. Hone, *NanoLett.*, 2008, 8, 982-987.
138P. Dong, C. L. Pint, M. Hainey, F. Mirri, Y. Zhu, J. Zhang, M. Pasquali, R. H. Hauge, R. Verduzco, M. Jiang, H. Lin and J. Luo, *ACS. Appl. Mater. Interfaces,* 2011, **3,** 3157-3161.
139E. G. Rakov, In Nanotubes and Nanofibers, Y. Gogoysi, Ed. Taylor & Francis: Newyork, 2006, 39.
140W. Lee, E. Ramasamy, D. Y. Lee and J. S. Song, *ACS Applied Materials and Interfaces*, 2009, **1**, 1145-1149.
141S. I. Cha, B. K. Koo, S. H. Seo and D. Y. Lee, *J. Mater. Chem*., 2010, **20**, 659-662.
142J. Han, H. Kim, D. Y. Kim, S. M. Jo and S. Y. Jang, *ACS Nano,* 2010, **4**, 3503-3509.
143S. Roy, R. Bajpai, A. Jena, P. Kumar, N. Kulshrestha and D.S. Misra, *Energy Environ. Sci*., 2012, **5**, 7001-7006.
144a)B. Fan, X. Mei, K. Sun and J. Ouyang, *Appl. Phys. Lett*., 2008, **93**, 2008, 143103.b) X. Sun, T. Chen, Z. Yang and H. Peng, *Accounts of chemical research*, 2013, **46**, 539-549.c) Z. Yang, T. Chen, R. He, G. Guan, H. Li, L. Qiu and H. Peng, *Adv. Mater*., 2011, **23**, 5436-5439.d) K.S. Lee, W. J. Lee, N. Park, *Chem. Commun*., 2011, **47**, 4264-4266.e)J. Velten, A. J. Mozer, D. Li, D. Officer, G. Wallace, R. Baughmam and A. Zakhidov, Nanotechnology, 2012, **23**, 85201-85207. f) F. malara, M. Manca, M. Lanza, C. Hubner, E. Piperopoulos and G. Gigli, Energy Environ. Sci., **5**, 8377-8383.
145A. K. Geim and K.S. Novoselov, *Nature Materials*, 2007, **6**, 183-191.
146S. Gilje, S. Han, M. Wang, K. L. Wang and R. B. Kaner, *Nano Lett*,2007, **7**, 3394-3398.
147D. Li and R. B. Kaner, *Science*, 2008, **320**, 1170-1171.
148X. Wang, L. Zhi and K. Mullen, *Nano Lett*, 2008, **8**, 323-327.
149H. Kim, H. Choi, S. Hwang, Y. Kim and M. Jeon, *Nanoscale Res Lett,* 2012, **7**, 53.
150C. T. Hsieh, B. H. Yang and J. Y. Lin, *Carbon*, 2011, **49**, 3092-3097.
151A. Kaniyoor & S.Ramprabhu, *J. Appl. Phys*., 2011, **109**, 124308.
152T. N. Murakami and M. Graztel, *Inorg Chim. Acta*, 2008, **361**, 572-580.
153C. E. Banks, T.J. Davies, G. G. Wildqoose and R. G. Compton, Chem. Commun., 2005, 829-841.
154L. Kavan, J. H. Yum and M. Graztel, *ACS Nano*, 2011, **5**, 165-172.
155J.D. Roy-Mayhew, D. J. Bozym, C. Punckt and I. A. Aksay, *ACS Nano*, 2010, **4**, 6203-6211
156L. S. Panchakarla, K.S. Subramanyam, S.K. Saha, Achutharao Govindaraj, H. R. Krishnamurthy, U. V. Waghmare and C. N. R. Rao, *Adv. Mater,*2009, **21**, 4726-4730.
157K. A. Kurak and A. B. Anderson, *J. Phys. Chem. C*, 2009, **113**, 6730-6734.
158M. J. Ju, J. C. Kim, H. J. Choi, S. G. Kim, K. Lim, J. Ko, J. J. Lee, I. Jeon, J. B. Baek and H. K. Kum, *ACS Nano*, 2013, **7**, 5243-5250.
159S. Stankovich, D. A. Dikin, G. H. B. Dommet, K. M. Kohlhass, E. J. Zimney, E. A. Stach, R. D. Piner, S. B. T. Nguyen and R. Ruoff, *Nature,* 2006, **442**, 282-286.
160W. Hong, Y. Xu, G. Lu, C. Li, G. Shi, *Electrochem. Commun*., 2008, **10**, 1555-1558.
161G. Wang, S. Zhuo, X. Wing, *Materials Letters*, 2012, **69**, 27-29.
162B. He, Q. Tang, M. Wang, H. Chen and S. Yuan, *ACS Appl. Mater. Interfaces*, 2014, **6**, 8230-8236.
163X. Xu, D. Huang, K. Cao, M. Wang, S. M. Zakeeruddin and M. Gratzel, *Scientific reports*, 2013, **3**, 1-7.
164S. P. Lim, A. Pandikumar, Y. S. Lim, N. M. Huang and H. N. Lim, *Scientific reports*, 2014, 4, 5305.
165T. Ma, X. Fang, M. Akiyama, K. Inoue, H. Noma, E. Abe, *J. Electroanal. Chem.,* 2004, **574**, 77-83.
166K. Miettunen, X. Ruan, T. Saukkonen, J. Halme, M. Toivola, H. Guangsheng and P. Lund, *J. Electrochem. Soc*., 2010, **157**, B814-B819.
167R. Bajpai, S. Roy, N. Kulshreshtha, J. Rafiee, N. Koratkar and D. S. Misra, *Nanoscale*, 2012, **4**, 926.
168V. Tjoa, J. Chua, S. S. Pramana, J. Wei, S. G. Mhaisalkar and N. Mathews, *ACS Appl. Mater. Interfaces*, 2012, **4**, 3447-3452.
169F. Gong, H. Wang and Z. S. Wang, Phys. Chem. Chem. Phys., 2011, **13**, 17676-17682.
170M. Wu, X. Lin, T. Wang, J. Qiu and T. Ma, *Energy Environ. Sci., 2011*, **4**, 2308-2315.
171Y. Y. Dou, G.R. Li, J. Song and X. P. Gao, *Phys. Chem. Chem. Phys.,* 2012, **14**, 1339-1342.
172K. Okada, H. Matsui, T. Kawashima, T. Ezure and N. Tanave, J. *Photochem.Photobiol.A*, 2004, **164**, 193-198.
173W.J. Lee, E. Ramasamy, D. Y. Lee and J. S. Song, *Sol.Energy. Mater.Sol.cells*, 2007, **91**, 1676-1680.
174T. Ma, X. Fang, M. Akiyama, K. Inoue, H. Noma and E. Abe, J. Electronal. Chem. 2004, **574**, 77-83.
175H. Lindstorm, A. Holmberg, E. Mangnusson, S. E. Lindquist, L. Malmqvist and A. Hagfeldt, NanoLett, 2001, **2**, 97-100.
176D.C. Zou, D. Wang, Z. Z. Chu, Z. B. Lv and X. Fan, *Coord.Chem.Rev*., 2010, **254**, 1169-1178.
177S. Hou, X. Cai, Y. Fu, Z. Lv, D. Wang, H. Wu, C. Zhang, Z. Chu and D. Zou, *J. Mater. Chem*., 2011, **21**, 13776.
178S. Zhang, C. Ji, Z. Bian, P. Zu, L. Zhang, D. Liu, E. Shi, Y. Shang, H. Peng, Q. cheng, D. Wang, C. Huang and A. Cao, *ACS Nano*, 2012, **6**, 7191-7198.
179S. Hou, X. Cai, H. Wu, Z. Lv, D. wang, Y. Fu and D. Zou, *J. of Power Sources*, 2012, **215**, 164-169.
180X. Cai, S. Hou, H. Wu, Z. Lv, Y. Fu, D. Wang, C. Zhang, H. Kafafy, Z. Chu and D. Zou, Phys. Chem. Chem. Phys., 2012, **14**, 125-130.
181T. Chen, L. Qiu, Z. Cai, F. Gong, Z. Yang, Z. Wang and H. Peng, *NanoLett*., 2012, **12**, 2568-2572.
182S. Pen, Z. Yang, P. Chen, X. Fang, G. Guan, Z. Zhang and H. Peng, J. Phys. Chem. C., 2014, **118**, 16419-16425.
183Q. Liu, Z. Liu, X. Zhang, L. Yang, N. Zhang, G. Pan, S. Yin, Y. Chen and J. Wei, *Adv. Funct. Mater*., 2009, **19**, 894-904.

184K. S. Novoselov, A. K. Geim, S.V. Morozov, Y. Zhang, S.V. Dubonos, I. V. Grigorieva, A.A. Firsov, *Science,* 2004, **306**, 666-669.
185X. Fang, M. Li, K. Guo, X. Liu, Y. Zhu, B. Sebo, X. Z. Zhao, Solar energy, 2014, **101**,176-181.
186H. Zhang, X. Lv, Y. Li, Y. Wang and J. Li, *ACS Nano*, 2010, 4, 380-386.
187C. B.Liu, Y. R. Teng, R. H.Liu, S. L. Luo, Y. H. Tang, L. Y. Chen, Q. Y. Cai, *Carbon*, 2011, **49**, 5312-5320.